Scheme 1. Synthesis of Amidine-Containing FC131 Analogue 15b

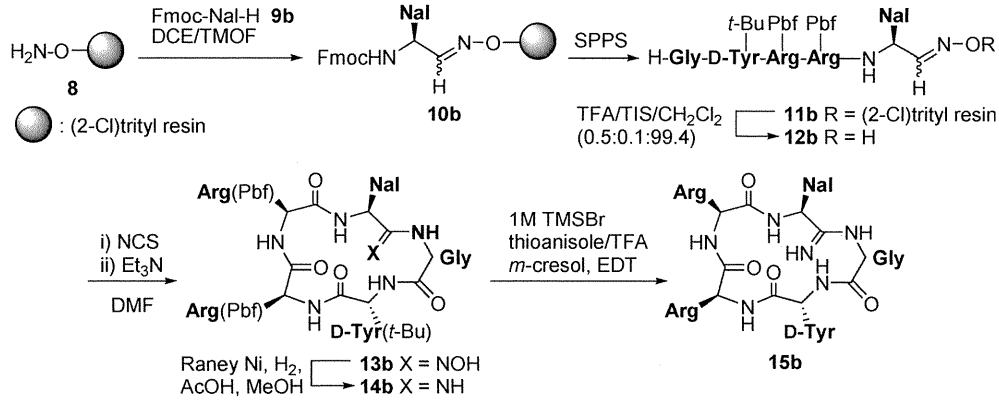

Table 2. Anti-HIV Activity of FC131 and the Derivatives 15a–g

	EC_{50} (nM)[a]		
peptide	NL4-3	IIIB	Ba-L
FC131 (2)	21 ± 4.3	21 ± 5.9	–[b]
FC122 (3)	7.6 ± 0.34	7.6 ± 1.1	–[b]
15a	1.3 ± 0.43	0.61 ± 0.10	–[b]
15b	1.4 ± 0.44	1.0 ± 0.23	–[b]
15c	2.2 ± 0.04	2.0 ± 0.59	–[b]
15d	4.4 ± 1.0	6.3 ± 0.47	–[b]
15e	1.9 ± 0.47	1.2 ± 0.29	–[b]
15f	300 ± 57	258 ± 47	–[b]
15g	248 ± 55	238 ± 37	–[b]

[a] EC_{50} is the concentration that blocks HIV-1 infection by 50%. [b] No inhibitory activity was observed at 10 μM.

the basicity. The partial double bond character of the amidine motif in **15d** might favorably constrain the cyclic configuration and place the side chains in the appropriate spatial orientations of the pharmacophore.

Recent reports of the docking model of FC131-CXCR4 interactions indicated that the amino group of the Gly-D-Tyr peptide bond forms a hydrogen bond to the carbonyl group of Ala95.[24,25] It was also suggested that the Arg-Arg dipeptide is surrounded by acidic residues in CXCR4 (Glu288 and Asp262).[24,25] The potent bioactivities of Gly-D-Tyr- and Arg-Arg-substituted analogues **15a** and **15e** may support the presence of these favorable interactions, which were enhanced by the introduction of positively charged amidine motifs. In particular, the amidine in the Arg-Arg dipeptide could form salt bridge(s) with the negatively charged residues.

Interestingly, both stereoisomers of Nal-Gly- and Tyr-Arg-modified analogues (**15b,c** and **15f,g**) showed similar antagonistic activities [**15b** (IC_{50} = 4.2 nM) and **15c** (IC_{50} = 4.9 nM); **15f** (IC_{50} = 679 nM) and **15g** (IC_{50} = 334 nM)]. This is in contrast to the suggestion that the bioactivity of FC131 derivatives is sensitive to the configurations of the component residues.[16,17] These results may suggest that the local conformation around the amidine motif is more flexible in cyclic pentapeptides than in the original peptide bond. Of note, none of the peptides **15a–g** showed inhibition against SDF-1-CXCR7 interaction (data not shown), which is reported to be an alternative receptor of SDF-1.

Anti-HIV activity based on inhibition of human immunodeficiency virus type 1 (HIV-1) entry into target cells was examined by the MAGI assay using NL4-3, IIIB, and Ba-L strains (Table 2). NL4-3 and IIIB strains use CXCR4 for entry into cells, and the FC131 analogues **15a–e** showed very potent anti-HIV activity against these strains. The two Tyr-Arg-substituted peptides **15f** and **15g** only moderately inhibited infection with these two strains, which was similar to their inhibitory effects against SDF-1-CXCR4 binding. The Ba-L strain uses CCR5 for entry to cells, and none of the peptides showed inhibitory activity against this strain even with the peptides at 10 μM. This result indicates that peptides **15a–g** show similar target specificity to FC131 as selective CXCR4 antagonists.[26] The cytotoxicity of analogues **15a–g** was not observed even at 10 μM in the MAGI assay.

In conclusion, we developed novel potent cyclic pentapeptide-based CXCR4 antagonists containing amidine type peptide bond isosteres. Substitutions of four peptide bonds in FC131, except for the D-Tyr-Arg position, with an amidine motif, improved the inhibitory activity against SDF-1 binding and HIV-1 infection by X4 strains. It was also demonstrated that the analogues were selective antagonists for CXCR4 and not for CXCR7 and CCR5, which are the targets shared by SDF-1 (CXCR7) and HIV-1 (CCR5). Further studies to understand the binding mode of these peptidomimetics and to develop derivatives with multiple amidine motifs in a single molecule are in progress.

■ ASSOCIATED CONTENT

Supporting Information. Experimental procedures and characterization data for all new compounds. This material is available free of charge via the Internet at http://pubs.acs.org.

■ AUTHOR INFORMATION

Corresponding Author

*Tel: +81-75-753-4551. Fax: +81-75-753-4570. E-mail: soishi@pharm.kyoto-u.ac.jp (S.O.) and nfujii@pharm.kyoto-u.ac.jp (N.F.).

Funding Sources

This work was supported by Grants-in-Aid for Scientific Research and Targeted Protein Research Program from MEXT and Health and Labor Science Research Grants (Research on HIV/AIDS, Japan).

E.I. was supported by a JSPS Research Fellowship for Young Scientists.

■ ABBREVIATIONS

CXCR4, CXC chemokine receptor type 4; HIV-1, human immunodeficiency virus type 1; Nal, 3-(2-naphthyl)alanine; DIC, *N,N'*-diisopropylcarbodiimide; HOBt, *N*-hydroxybenzotriazole; SDF-1, stromal cell-derived factor 1

■ REFERENCES

(1) Loetscher, M.; Geiser, T.; O'Reilly, T.; Zwahlen, R.; Baggiolini, M.; Moser, B. Cloning of a human seven-transmenbrane domain receptor, LESTR, that is highly expressed in leukocytes. *J. Biol. Chem.* **1994**, *269*, 232–237.

(2) Nagasawa, T.; Kikutani, H.; Kishimoto, T. Molecular cloning and structure of a pre-B-cell growth-stimulating factor. *Proc. Natl. Acad. Sci. U.S.A.* **1994**, *91*, 2305–2309.

(3) Müller, A.; Homey, B.; Soto, H.; Ge, N.; Catron, D.; Buchanan, M. E.; McClanahan, T.; Murphy, E.; Yuan, W.; Wagner, S. N.; Barrera, J. L.; Mohar, A.; Verástegui, E.; Zlotnik, A. Involvement of chemokine receptors in breast cancer metastasis. *Nature* **2001**, *410*, 50–56.

(4) Feng, Y.; Broder, C. C.; Kennedy, P. E.; Berger, E. A. HIV-1 entry cofactor: functional cDNA cloning of a seven-transmembrane, G protein-coupled receptor. *Science* **1996**, *272*, 872–877.

(5) O'Hayre, M.; Salanga, C. L.; Handel, T. M.; Hamel, D. Emerging concepts and approaches for chemokine-receptor drug discovery. *Expert Opin. Drug Discovery* **2010**, *5*, 1109–1122.

(6) Tamamura, H.; Xu, Y.; Hattori, T.; Zhang, X.; Arakaki, R.; Kanbara, K.; Omagari, A.; Otaka, A.; Ibuka, T.; Yamamoto, N.; Nakashima, H.; Fujii, N. A low-molecular-weight inhibitor against the chemokine receptor CXCR4: A strong anti-HIV peptide T140. *Biochem. Biophys. Res. Commun.* **1998**, *253*, 877–882.

(7) Bridger, G. J.; Skerlj, R. T.; Thornton, D.; Padmanabhan, S.; Martellucci, S. A.; Henson, G. W.; Abrams, M. J.; Yamamoto, N.; De Vreese, K.; Pauwels, R.; De Clercq, E. Synthesis and structure−activity relationships of phenylenebis(methylene)-linked bis-tetraazamacrocycles that inhibit HIV replication. Effects of macrocyclic ring size and substituents on the aromatic linker. *J. Med. Chem.* **1995**, *38*, 366–378.

(8) Doranz, B. J.; Grovit-Ferbas, K.; Sharron, M. P.; Mao, S.-H.; Bidwell Goetz, M.; Daar, E. S.; Doms, R. W.; O'Brien, W. A. A small-molecule inhibitor directed against the chemokine receptor CXCR4 prevents its use as an HIV-1 coreceptor. *J. Exp. Med.* **1997**, *186*, 1395–1400.

(9) Bridger, G. J.; Skerlj, R. T.; Hernandez-Abad, P. E.; Bogucki, D. E.; Wang, Z.; Zhou, Y.; Nan, S.; Boehringer, E. M.; Wilson, T.; Crawford, J.; Metz, M.; Hatse, S.; Princen, K.; De Clercq, E.; Schols, D. Synthesis and structure−activity relationships of azamacrocyclic C-X-C chemokine receptor 4 antagonists: Analogues containing a single azamacrocyclic ring are potent inhibitors of T-cell tropic (X4) HIV-1 replication. *J. Med. Chem.* **2010**, *53*, 1250–1260.

(10) Skerlj, R. T.; Bridger, G. J.; Kaller, A.; McEachern, E. J.; Crawford, J. B.; Zhou, Y.; Atsma, B.; Langille, J.; Nan, S.; Veale, D.; Wilson, T.; Harwig, C.; Hatse, S.; Princen, K.; De Clercq, E.; Schols, D. Discovery of novel small molecule orally bioavailable C-X-C chemokine receptor 4 antagonists that are potent inhibitors of T-tropic (X4) HIV-1 replication. *J. Med. Chem.* **2010**, *53*, 3376–3388.

(11) Zhan, W.; Liang, Z.; Zhu, A.; Kurtkaya, S.; Shim, H.; Snyder, J. P.; Liotta, D. C. Discovery of small molecule CXCR4 antagonists. *J. Med. Chem.* **2007**, *50*, 5655–5664.

(12) Rosenkilde, M. M.; Gerlach, L.-O.; Jakobsen, J. S.; Skerlj, R. T.; Bridger, G. J.; Schwartz, T. W. Molecular mechanism of AMD3100 antagonism in the CXCR4 receptor. *J. Biol. Chem.* **2004**, *279*, 3033–3041.

(13) Zhang, W.; Navenot, J.-M.; Haribabu, B.; Tamamura, H.; Hiramatsu, K.; Omagari, A.; Pei, G.; Manfredi, J. P.; Fujii, N.; Broach, J. R.; Peiper, S. C. A point mutation that confers constitutive activity to CXCR4 reveals that T140 is an inverse agonist and that AMD3100 and ALX40-4C are weak partial agonists. *J. Biol. Chem.* **2002**, *277*, 24515–24521.

(14) Wu, B.; Chien, E. Y. T.; Mol, C. D.; Fenalti, G.; Liu, W.; Katritch, V.; Abagyan, R.; Brooun, A.; Wells, P.; Bi, F. C.; Hamel, D. J.; Kuhn, P.; Handel, T. M.; Cherezov, V.; Stevens, R. C. Structures of the CXCR4 chemokine GPCR with small-molecule and cyclic peptide antagonists. *Science* **2010**, *330*, 1066–1071.

(15) Fujii, N.; Oishi, S.; Hiramatsu, K.; Araki, T.; Ueda, S.; Tamamura, H.; Otaka, A.; Kusano, S.; Terakubo, S.; Nakashima, H.; Broach, J. A.; Trent, J. O.; Wang, Z.; Peiper, S. C. Molecular-size reduction of a potent CXCR4-chemokine antagonist using orthogonal combination of conformation- and sequence-based libraries. *Angew. Chem., Int. Ed.* **2003**, *42*, 3251–3253.

(16) Ueda, S.; Oishi, S.; Wang, Z.; Araki, T.; Tamamura, H.; Cluzeau, J.; Ohno, H.; Kusano, S.; Nakashima, H.; Trent, J. O.; Peiper, S. C.; Fujii, N. Structure−activity relationships of cyclic peptide-based chemokine receptor CXCR4 antagonists: disclosing the importance of side-chain and backbone functionalities. *J. Med. Chem.* **2007**, *50*, 192–198.

(17) Tamamura, H.; Araki, T.; Ueda, S.; Wang, Z.; Oishi, S.; Esaka, A.; Trent, J. O.; Nakashima, H.; Yamamoto, N.; Peiper, S. C.; Otaka, A.; Fujii, N. Identification of novel low molecular weight CXCR4 antagonists by structural tuning of cyclic tetrapeptide scaffolds. *J. Med. Chem.* **2005**, *48*, 3280–3289.

(18) Tamamura, H.; Hiramatsu, K.; Ueda, S.; Wang, Z.; Kusano, S.; Terakubo, S.; Trent, J. O.; Peiper, S. C.; Yamamoto, N.; Nakashima, H.; Otaka, A.; Fujii, N. Stereoselective synthesis of [L-Arg-L/D-3-(2-naphthyl)alanine]-type (*E*)-alkene dipeptide isosteres and its application to the synthesis and biological evaluation of pseudopeptide analogues of the CXCR4 antagonist FC131. *J. Med. Chem.* **2005**, *48*, 380–391.

(19) Narumi, T.; Hayashi, R.; Tomita, K.; Kobayashi, K.; Tanahara, N.; Ohno, H.; Naito, T.; Kodama, E.; Matsuoka, M.; Oishi, S.; Fujii, N. Synthesis and biological evaluation of selective CXCR4 antagonists containing alkene dipeptide isosteres. *Org. Biomol. Chem.* **2010**, *8*, 616–621.

(20) Inokuchi, E.; Yamada, A.; Hozumi, K.; Tomita, K.; Oishi, S.; Ohno, H.; Nomizu, M.; Fujii, N. *Org. Biomol. Chem.* **2011**, DOI: 10.1039/c0ob01193b.

(21) Moser, H.; Fliri, A.; Steiger, A.; Costello, G.; Schreiber, J.; Eschenmoser, A. Poly(dipeptamidinium) salts: Definition and methods of preparation. *Helv. Chim. Acta* **1986**, *69*, 1224–1262.

(22) Jones, R. C. F.; Ward, G. J. Amide bond isosteres: imidazolines in pseudopeptide chemistry. *Tetrahedron Lett.* **1988**, *29*, 3853–3856.

(23) Epimerizations in the preparation of protected cyclic peptides **13b** and **13f** were verified by the comparative HPLC analysis of the amidine isomers **14b/14c** and the amidoxime isomers **13f/13g**, respectively (**14b**, 90% *de*; **13f**, 95% *de*; see the Supporting Information for details).

(24) Våbenø, J.; Nikiforovich, G. V.; Marshall, G. R. A minimalistic 3D pharmacophore model for cyclopentapeptide CXCR4 antagonists. *Biopolymers* **2006**, *84*, 459–471.

(25) Våbenø, J.; Nikiforovich, G. V.; Marshall, G. R. Insight into the binding mode for cyclopentapeptide antagonists of the CXCR4 receptor. *Chem. Biol. Drug Des.* **2006**, *67*, 346–354.

(26) Oishi, S.; Masuda, R.; Evans, B.; Ueda, S.; Goto, Y.; Ohno, H.; Hirasawa, A.; Tsujimoto, G.; Wang, Z.; Peiper, S. C.; Naito, T.; Kodama, E.; Matsuoka, M.; Fujii, N. Synthesis and application of fluorescein- and biotin-labeled molecular probes for the chemokine receptor CXCR4. *ChemBioChem* **2008**, *9*, 1154–1158.

blood

2011 118: 1865-1876
Prepublished online June 24, 2011;
doi:10.1182/blood-2010-12-326199

HTLV-1 bZIP factor enhances TGF-β signaling through p300 coactivator

Tiejun Zhao, Yorifumi Satou, Kenji Sugata, Paola Miyazato, Patrick L. Green, Takeshi Imamura and Masao Matsuoka

Blood (print ISSN 0006-4971, online ISSN 1528-0020), is published weekly by the American Society of Hematology, 2021 L St, NW, Suite 900, Washington DC 20036.

HTLV-1 bZIP factor enhances TGF-β signaling through p300 coactivator

Tiejun Zhao,[1] Yorifumi Satou,[1] Kenji Sugata,[1] Paola Miyazato,[1] Patrick L. Green,[2] Takeshi Imamura,[3-5] and Masao Matsuoka[1]

[1]Laboratory of Virus Control, Institute for Virus Research, Kyoto University, Kyoto, Japan; [2]Center for Retrovirus Research and Departments of Veterinary Biosciences and Molecular Virology, Immunology and Medical Genetics, The Ohio State University, Columbus, OH; [3]Department of Molecular Medicine for Pathogenesis, Ehime University Graduate School of Medicine, Ehime, Japan; [4]Division of Biochemistry, Cancer Institute of the Japanese Foundation for Cancer Research, Tokyo, Japan; and [5]Core Research for Evolutional Science and Technology, Japan Science and Technology Agency, Tokyo, Japan

Human T-cell leukemia virus type 1 (HTLV-1) is an oncogenic retrovirus that is etiologically associated with adult T-cell leukemia. The HTLV-1 bZIP factor (HBZ), which is encoded by the minus strand of the provirus, is involved in both regulation of viral gene transcription and T-cell proliferation. We showed in this report that HBZ interacted with Smad2/3, and enhanced transforming growth factor-β (TGF-β)/Smad transcriptional responses in a p300-dependent manner. The N-terminal LXXLL motif of HBZ was responsible for HBZ-mediated TGF-β signaling activation. In a serial immunoprecipitation assay, HBZ, Smad3, and p300 formed a ternary complex, and the association between Smad3 and p300 was markedly enhanced in the presence of HBZ. In addition, HBZ could overcome the repression of the TGF-β response by Tax. Finally, HBZ expression resulted in enhanced transcription of *Pdgfb*, *Sox4*, *Ctgf*, *Foxp3*, *Runx1*, and *Tsc22d1* genes and suppression of the *Id2* gene; such effects were similar to those by TGF-β. In particular, HBZ induced Foxp3 expression in naive T cells through Smad3-dependent TGF-β signaling. Our results suggest that HBZ, by enhancing TGF-β signaling and Foxp3 expression, enables HTLV-1 to convert infected T cells into regulatory T cells, which is thought to be a critical strategy for virus persistence. (*Blood*. 2011;118(7):1865-1876)

Introduction

Human T-cell leukemia virus type 1 (HTLV-1) is the etiologic agent of adult T-cell leukemia (ATL) and HTLV-1–associated myelopathy/tropical spastic paraparesis (HAM/TSP).[1,2] The unique sequence of HTLV-1 between the *env* region and 3′ long terminal repeat, denoted the pX region, encodes regulatory (*tax* and *rex*) and accessory (*p12*, *p13*, and *p30*) genes in the plus strand.[3] The pleiotropic actions of Tax are thought to play a central role in the early stage of leukemogenesis.[4] However, approximately 60% of fresh ATL cells lack Tax expression because of genetic and epigenetic changes in the HTLV-1 provirus, suggesting that Tax may not be essential for the maintenance of ATL cells in vivo.[5] The *HTLV-1 bZIP factor* (*HBZ*), which is encoded by the complementary strand of the HTLV-1 genome, is expressed in all ATL cases and supports the proliferation of ATL cells.[6,7] In addition, HBZ was found to inhibit Tax-mediated activation of viral transcription from the 5′-long terminal repeat by heterodimerizing with c-Jun, CREB2, and to selectively suppress the classic pathway of nuclear factor-κB by 2 distinct mechanisms.[8-11] Thus, HBZ has multifunctional roles in cellular signaling and proliferation. Recently, we reported that nonsense mutations in all HTLV-1 genes except *HBZ* were generated by APOBEC3G before integration of the provirus in ATL cases and HTLV-1 infected persons, indicating that the *HBZ* gene is essential for leukemogenesis.[12]

Transforming growth factor-β (TGF-β) controls a variety of biologic processes, including cell growth, differentiation, apoptosis, development, and immune homeostasis.[13] The Smad proteins, which are mediators of TGF-β signaling, transduce the TGF-β signal at the cell surface into gene regulation in the nucleus. Receptor-regulated Smad, R-Smads (Smad1, 2, 3, 5, and 8), are phosphorylated by the activated TGF-β receptor, form complexes with Comediator Smad, Co-Smad (Smad 4), and together accumulate in the nucleus to regulate transcription of target genes. Smads can regulate gene expression positively by recruiting coactivators, such as CBP/p300,[14] or negatively by direct recruitment of histone deacetylases or corepressors, such as c-Ski and SnoN.[15] In ATL cells, constitutively activated AP-1 leads to the production of TGF-β1,[16] which can be readily detected in the serum of infected persons.[17] Subsequent studies reported that HTLV-1–infected T cells were resistant to TGF-β–induced growth inhibition and that resistance was related to Tax expression. Three distinct mechanisms by which Tax suppressed TGF-β–mediated signaling were reported: (1) inhibition of Smad3-Smad4 complex formation and DNA binding; (2) prevention of the recruitment of CBP/p300 to the Smad transcription complex on TGF-β response elements; and (3) inhibition of Smad3 DNA binding through activation of the JNK/c-Jun pathway.[18-20]

TGF-β signaling is critical for the development of $CD4^+CD25^+Foxp3^+$ regulatory T cells (Tregs).[21] ATL cells possess a $CD4^+CD25^+$ phenotype, similar to that of Tregs. The forkhead box P3 (FoxP3) is critical for the function of Tregs.[22] Expression of FoxP3 was detected in two-thirds of ATL cases,[23] indicating that ATL cells are derived from Tregs, and a recent study reported a higher proportion of $FoxP3^+$ Tregs among the HTLV-1–infected cells than among the HTLV-1–negative $CD4^+$ cells.[24] Although Tax has been reported to suppress FoxP3 expression in T cells,[25] we recently found that HBZ expression-induced Foxp3

Submitted December 20, 2010; accepted June 5, 2011. Prepublished online as *Blood* First Edition paper, June 24, 2011; DOI 10.1182/blood-2010-12-326199.

The online version of this article contains a data supplement.

The publication costs of this article were defrayed in part by page charge payment. Therefore, and solely to indicate this fact, this article is hereby marked "advertisement" in accordance with 18 USC section 1734.

expression and increased the number of Tregs.[26] Therefore, we set out to determine how HBZ and TGF-β cooperate to induce FoxP3 in HTLV-1–infected T cells.

In the present study, we found that HBZ enhanced TGF-β signaling by interacting with Smad3 and p300, resulting in enhanced Foxp3 expression. This might account for why HTLV-1 infection increases Tregs in vivo.

Methods

Cell culture and mice

HTLV-1 immortalized cell lines (MT-2, MT-4), ATL cell lines (MT-1, ATL-2, ATL-T, ATL-43T, ATL-55T, ED, and TL-Oml), T-cell lines not infected with HTLV-1 (Jurkat, Hut78, CEM, and Kit 225), and mouse T-cell line (CTLL-2) were maintained as described previously.[27] HepG2, 293T, and COS7 cells were grown in Dulbecco modified Eagle medium supplemented with 10% FBS and antibiotics. Plat-E cells were cultured in Dulbecco modified Eagle medium supplemented with 10% FBS containing 10 μg/mL blasticidin and 1 μg/mL puromycin. EL4 cells were cultured with RPMI 1640 containing 10% FCS, antibiotics, and 50μM 2-mercaptoethanol. C57BL/6J mice were purchased from CLEA Japan. Peripheral blood mononuclear cells were isolated from healthy volunteers under an institutional review board-approved protocol. All animals used in this study were maintained and handled according to protocols approved by Kyoto University.

Plasmids

The 3TP-Lux construct contains the phorbol myristate acetate-response elements along with the Smad3/4 binding sites of the PAI-1 promoter. A total of 9 × CAGA-Luc contains 9 tandem Smad3/4 binding sites. pTARE-Luc was purchased from Stratagene. phRL-TK was purchased from Promega. Expression plasmids for Tax, spliced HBZ (sHBZ), unspliced HBZ (usHBZ), c-Ski, Smads, and their deletion mutants were prepared as previously described.[11,28] Expression vectors for sHBZ-ΔbZIP deletion mutants were generated by polymerase chain reaction (PCR). The coding region of c-Fos was amplified by reverse-transcribed (RT)-PCR from total RNA derived from primary peripheral blood mononuclear cells and cloned into the vector pCDNA3. Expression plasmids for E1A and its mutants were a gift from Dr Akiyoshi Fukamizu of University of Tsukuba, and pEF-HA-p300 was from Dr Takashi Fujita of Kyoto University. The STAT5-responsive Jγ1 promoter reporter plasmid (pGL4-Jγ1), pCAGGS-WT-STAT5a (wild-type), and pCAGGS-CA-STAT5a (constitutively active) were provided by Dr Koichi Ikuta of Kyoto University.

Luciferase assay

HepG2 cells were plated on 12-well plates at 2.5×10^5 cells per well. After 24 hours, cells were transfected with the indicated plasmid. At 48 hours after transfection, a luciferase reporter assay was performed as previously described.[11] For CTLL-2 cells, vectors were transfected with a Gene Pulser II electroporation system (Bio-Rad). The transfected cells were treated with or without 10 ng/mL TGF-β (RD Systems) for 24 hours before being harvested for the reporter assay. For the Foxp3 reporter assay, the *Foxp3* gene promoter and enhancer were cloned into the pGL4.1 basic vector as previously reported.[29] Mutations of the Smad binding site in the enhancer fragment were generated by PCR. Foxp3 reporter assays were performed in EL4 cells as described.[29] Each experiment was performed in triplicate, and the data represent the mean plus or minus SD of 3 independent experiments, each normalized to *Renilla* activity.

Immunoprecipitation and immunoblotting

HepG2 and COS7 cells were transfected with the indicated plasmids by *Trans*IT-LT1 (Mirus). Tagged proteins were isolated from transfected COS7 cells by immunoprecipitation with anti–c-Myc (clone 9E10, Sigma-Aldrich), anti-HA (12CA5, Roche Diagnostics) or anti-FLAG M2 (Sigma-Aldrich) antibodies, and analyzed by Western blot as described previously.[11]

For sequential immunoprecipitation, transfected COS7 cells were lysed in radioimmunoprecipitation assay buffer and immunoprecipitated with anti-FLAG M2 agarose affinity gel. The precipitates were eluted with FLAG peptide and the eluate diluted with radioimmunoprecipitation assay buffer, immunoprecipitated with anti-HA antibody, and subjected to anti-His (MBL) immunoblotting. Membranes were developed by enhanced chemiluminescence (GE Healthcare Life Sciences). Other antibodies used were as follows: anti–mouse immunoglobulin G (IgG), and anti–rabbit IgG were from GE Healthcare Life Sciences; anti-Smad3 was from ZYMED Laboratories (Zymed); and anti-HBZ was used as previously described.[30]

Immunofluorescence analysis

COS7 cells were transfected with expression vectors using *Trans*IT-LT1 and treated with TGF-β (5 ng/mL) for 2 hours. At 48 hours after transfection, sHBZ protein was detected using anti–c-MYC Cy3 (clone 9E10, Sigma-Aldrich). Smad3 was detected using anti–FLAG-biotin (Sigma-Aldrich) and secondary streptavidin-Alexa-488 antibody (Invitrogen). Fluorescence was observed with a 63×/1.4-0.60 HCX PL APO objective on a DMIRE2-TCS AOBS confocal microscope system (Leica). Images were acquired and analyzed using LCS 2.61 (Leica) and processed using Photoshop CS2 (Adobe Systems).

ChIP assay

HepG2 cells were transfected with the indicated expression vectors together with 3TP-Lux reporter plasmid. At 24 hours after transfection, cells were treated with TGF-β (5 ng/mL). At 48 hours after transfection, ChIP assay was done according to the protocol recommended by Upstate Biotechnology. Precipitated DNA was amplified by PCR using primers specific for 3TP-Lux vector. Sequences for the primer set were 5′-CCCCCTGAACCTGAAACATA-3′ and 5′-CCTGAGGGCTCTCTTGTGTC-3′. For the endogenous *FoxP3* enhancer, chromatin samples prepared from MT-2 cells treated with 5 ng/mL of TGF-β for 2 hours were subjected to ChIP analysis using the following antibodies: anti-HBZ,[31] anti-Smad3 (BD Biosciences), anti-p300 (Santa Cruz Biotechnology), and normal mouse or rabbit immunoglobulin G (Santa Cruz Biotechnology). Primers used were 5′-CCTATGTTGGCTTCTAGTCTCTTTTATGG-3′ and 5′-TATGGAGAGGTTAAGTGCCTGGCTA-3′.

Synthesis of cDNA and semiquantitative RT-PCR

Total RNA was isolated using Trizol Reagent (Invitrogen) according to the manufacturer's instructions. We reverse-transcribed 1 μg of total RNA into single-stranded cDNA with SuperScript II reverse transcriptase (Invitrogen). Using forward (F) and reverse (R) primers specific to the target genes, the cDNA was amplified by increasing PCR cycles. The specific primers used can be found in supplemental Table 1 (available on the *Blood* Web site; see the Supplemental Materials link at the top of the online article).

Transfection and cell proliferation assay

Expression and control vectors were transfected into CTLL-2 cells by electroporation, and those cells were selected by G418 (0.5 mg/mL). Two transfectants, CTLL-2/pME18Sneo and CTLL-2/sHBZ, were established. For cell proliferation studies, sHBZ-expressing CTLL-2 and the control cells were plated at a density of 1×10^4 cells/well in 96-well plates. Cells were treated with increasing concentrations of TGF-β for 72 hours and assayed for cell growth by the methyl thiazolyl tetrazolium assay. Each experiment was performed 3 times, and representative results are presented.

Retroviral constructs and transduction

sHBZ cDNA was cloned into the retroviral vectors, pGCDNsamI/N and pMXs-IG, to generate pGCDNsamI/N-sHBZ and pMXs-sHBZ-IG. Transfection of the packaging cell line, Plat-E, was performed as described.[32] Mouse splenocytes were enriched for $CD25^-CD4^+$ cells with a CD4 T lymphocyte enrichment set (BD Biosciences) with the addition of

biotinylated anti-CD25 antibody (BD Biosciences), and activated by antigen-presenting cells (T cell-depleted and X-irradiated (20 Gy) C57BL/6J splenocytes) in the presence of 0.5 μg/mL anti-CD3 antibody and 50 U/mL human recombinant IL-2 in 12-well plates. After 24 hours, activated T cells were transduced with viral supernatant and 4 μg/mL polybrene, and centrifuged at 1700*g* for 60 minutes. Cells were subsequently cultured in medium supplemented with 50 U/mL recombinant IL-2.

Lentiviral vector construction and transfection of recombinant lentivirus

We cloned sHBZ cDNA into the *Eco*RI site of a lentiviral vector, pCSII-EF-MCS. The IRES-NGFR cassette was inserted into the *Xba*I site, which is located downstream of the sHBZ gene. Lentiviral vectors were produced as described.[7] Human peripheral blood mononuclear cells were enriched for $CD4^+CD25^-$ cells with a human naive CD4 T-cell enrichment set (BD Biosciences) and activated by anti-CD3/28–coated beads (Invitrogen). After 24 hours, cells were incubated with concentrated vector stocks in the presence of 4 μg/mL polybrene.

Flow cytometric analysis

Cells were washed with phosphate-buffered saline containing 1% FBS. After centrifugation, cells were treated with AlexaFluor-467–conjugated anti–human NGFR antibody (BD Biosciences) for 30 minutes. Cells were fixed and permeabilized at 4°C overnight and then treated with eFluor 450 conjugated anti-Foxp3 antibody (eBioscience) at 4°C for 30 minutes. After being washed with PBS, the cells were analyzed with a flow cytometer (BD FACSCanto II, BD Biosciences).

Cell sorting

Mouse naive T cells transduced with viral supernatant derived from the pMXs-sHBZ-IG and pMXs-IG vectors were sorted for the expression of green fluorescent protein using a FACSAria with Diva software (BD Biosciences PharMingen).

Statistical analyses

Statistical analyses were performed using the unpaired Student *t* test.

Results

HBZ protein enhances TGF-β/Smad–mediated signaling

To analyze the effect of HBZ on TGF-β–mediated transcriptional responses, HepG2 cells were cotransfected with an HBZ expression vector along with different TGF-β responsive reporters: TARE-Luc, 3TP-Lux, and 9 × CAGA-Luc. As shown in Figure 1A-C, sHBZ enhanced the transcription of luciferase in each of the reporter plasmid DNAs. sHBZ also up-regulated TGF-β transcription in a mouse T-cell line, CTLL-2 (Figure 1D). TGF-β signaling was increasingly activated when less than 200 ng of sHBZ expression vector, pcDNA3.1-mycHis-sHBZ, was added to each well. At higher levels (> 200 ng) of sHBZ plasmid DNA, however, activation of TGF-β signaling partially decreased (Figure 1E). In addition, pME18Sneo-based sHBZ vector activated TGF-β signaling with the same tendency as pcDNA3.1-mycHis-sHBZ did, whereas 20 ng of pME18Sneo-sHBZ plasmid was sufficient for maximal activation (supplemental Figure 1).

HBZ interacts with Smads

To clarify the molecular mechanism by which HBZ enhances the TGF-β transcriptional response, FLAG-tagged Smad2, Smad3, Smad4, or Smad7 and mycHis-tagged sHBZ were cotransfected into COS7 cells. Figure 2A demonstrates that sHBZ interacted with Smad2/3 and, to a lesser extent, with Smad4. TGF-β treatment had little effect on these interactions. Because a high degree of homology exists between Smad2 and Smad3, our subsequent analyses focused on the Smad3-HBZ interaction. We next examined the subcellular localization of sHBZ and Smad3 by confocal microscopy. After stimulating with TGF-β, cotransfected cells showed nuclear spots representing colocalization of sHBZ and Smad3 (Figure 2B). Activated Smad3 forms heteromeric complexes with the Co-Smad, Smad4, and translocates to the nucleus where it directly regulates transcription of target genes.[15] We therefore investigated whether HBZ influenced Smad3/Smad4 complex formation. COS7 cells were transfected with 6myc-Smad4 and FLAG-Smad3 with or without sHBZ. As shown in Figure 2C, sHBZ did not influence interaction between Smad3 and Smad4.

HBZ depends on the coactivator p300 to enhance TGF-β–mediated transcription

To address whether p300 is functionally required for the enhancement of TGF-β–mediated transcription by HBZ, we evaluated the effect of the adenovirus E1A oncoprotein,[33] an inhibitor of p300 activity, on the ability of HBZ to enhance TGF-β transcriptional activity. As shown in Figure 3A, wild-type E1A significantly suppressed the ability of TGF-β and sHBZ to enhance transcriptional activity through Smad-responsive elements, whereas a mutant form of E1A, E1A-ΔNT, which is defective for p300/CBP binding, had no effect on these responses. Moreover, in the presence of p300, sHBZ dramatically up-regulated Smad3-mediated TGF-β activation, whereas it had a less obvious effect without p300. This synergistic effect of HBZ and p300 on TGF-β activation was augmented with TGF-β treatment (Figure 3B).

As HBZ enhanced p300 and Smad3's activation of TGF-β signaling, we next explored whether HBZ, Smad3, and p300 could form a ternary complex. The plasmid DNAs, mycHis-sHBZ, FLAG-Smad3, and HA-p300 were cotransfected into COS7 cells that were then treated with or without TGF-β. FLAG-Smad3 and its associated proteins were immunoprecipitated using anti-FLAG, eluted with FLAG peptide, and subjected to a second immunoprecipitation with anti-HA antibody. The anti-HA immunoprecipitates were then subjected to Western blot analysis with anti-His antibody. As shown in Figure 3C, we detected a specific ternary complex only when the 3 components were coexpressed, which was enhanced in the presence of TGF-β. Furthermore, sHBZ protein greatly enhanced the interaction between Smad3 and p300 (Figure 3D). To investigate the binding of sHBZ/Smad3/p300 to DNA, we performed ChIP assay in HepG2 cells that were cotransfected with 3TP-Lux reporter along with expression vectors of sHBZ, Smad3, and p300. The ChIP assay detected the association of each of 3 proteins with Smad responsive elements, which indicated that sHBZ was recruited to 3TP promoter through forming complex with Smad3/p300. Akiyoshi et al reported that c-Ski counteracted p300 and acted as a transcriptional corepressor for Smads in the TGF-β signaling pathway.[34] Therefore, we studied whether HBZ could affect the interaction between Smad3 and c-Ski and found that sHBZ did not interfere with the formation of Smad3/c-Ski complex (supplemental Figure 2). These results together suggest that HBZ augments the interaction between Smad3 and p300, thereby potentiating TGF-β signaling.

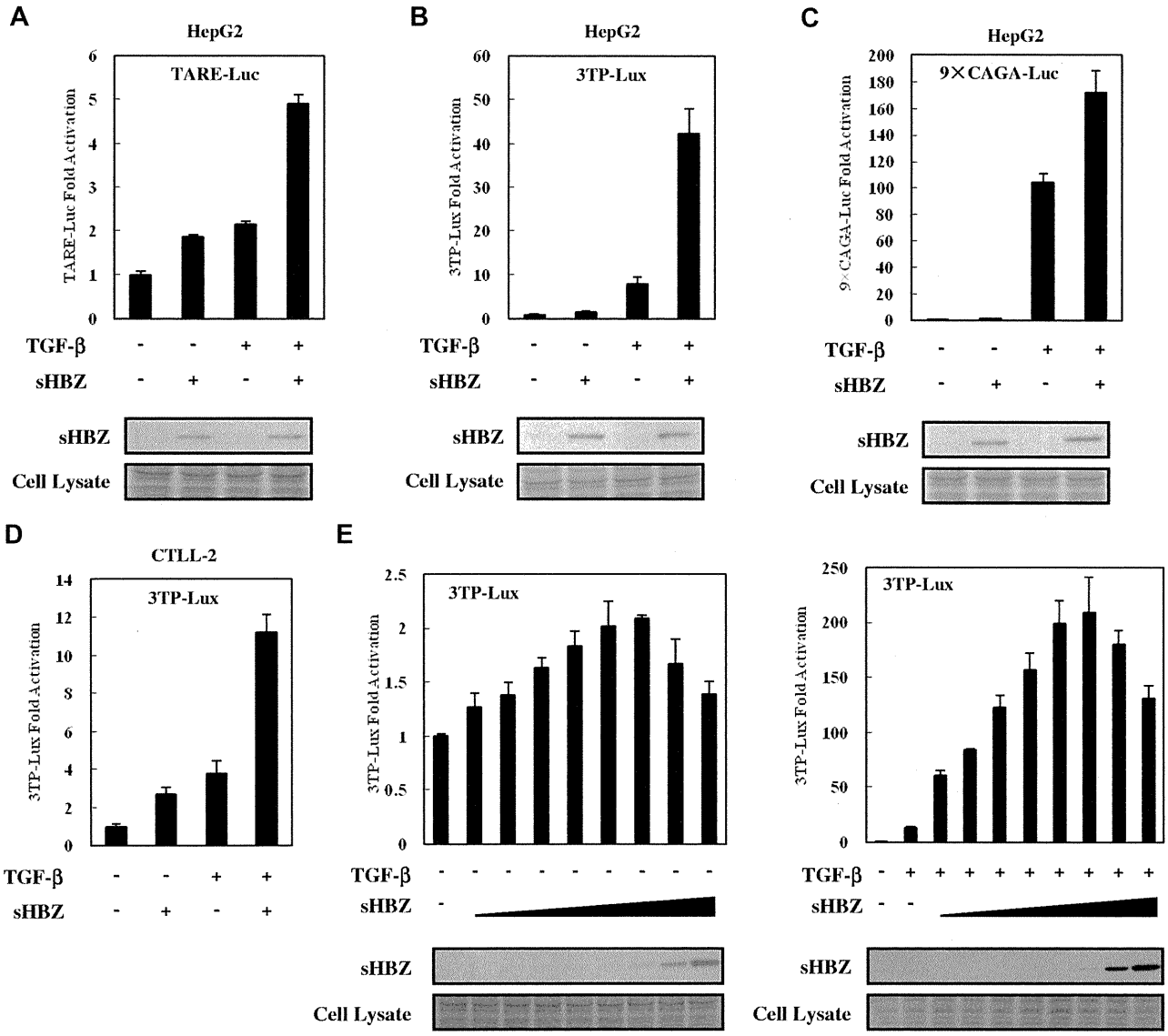

Figure 1. HBZ activated TGF-β signaling. In 12-well plates, HepG2 cells were cotransfected with 2 ng of phRL-TK, 0.5 μg of reporter plasmid TARE-Luc (A), 3TP-Lux (B), or 9 × CAGA-Luc (C), and 0.5 μg of pcDNA3.1-mycHis-sHBZ. At 24 hours after transfection, the cells were treated with TGF-β (10 ng/mL). After 24 hours, the cells were harvested and analyzed for luciferase activity. Expression of sHBZ was detected by Western blot (middle panel). Coomassie brilliant blue (CBB) staining was shown as the loading control (botom panel). (D) CTLL-2 cells were transfected with 3TP-Lux (2 μg), phRL-TK (10 ng), and pME18Sneo-sHBZ (0.4 μg) by electroporation. Luciferase activity was measured 24 hours after stimulation by TGF-β. (E) In 12-well plates, HepG2 cells were cotransfected with 3TP-Lux (0.5 μg), phRL-TK (2 ng), and pcDNA3.1-mycHis-sHBZ (0, 5, 10, 20, 50, 100, 200, 1000, and 4000 ng). At 24 hours after transfection, the cells were treated with or without TGF-β. After 24 hours, the cells were harvested and analyzed for luciferase activity. mycHis-sHBZ was detected by Western blot (middle panel). CBB staining was shown as the loading control (bottom panel).

Domains of HBZ responsible for enhancement of TGF-β–mediated transcription

Two major isoforms of the *HBZ* gene have been reported: spliced (s*HBZ*) and unspliced (us*HBZ*) *HBZ* (Figure 4A left panel). usHBZ caused a similar activation of TGF-β responses to that caused by sHBZ (Figure 4A right panel). We next evaluated the sHBZ deletion mutants shown in Figure 4B to determine which region of HBZ is responsible for activating TGF-β signaling. Three mutants (sHBZ-AD, sHBZ-ΔbZIP, and sHBZ-AD+bZIP) enhanced the response to TGF-β, whereas the sHBZ-bZIP mutant exhibited only suppressive activity (Figure 4C). The sHBZ-ΔbZIP mutant, which maintains the central domain (CD) and the activation domain (AD), had a dramatically reinforced activation capacity compared with sHBZ-AD; however, the central domain alone (sHBZ-ΔADΔbZIP mutant) did not influence TGF-β. The sHBZ-AD+bZIP mutant displayed a similar effect to that of wild-type sHBZ (Figure 1E; Figure 4C). These results indicate that the AD domain of HBZ is responsible for the activation of TGF-β signaling whereas bZIP domain shows a suppressive effect.

To determine the precise region within the AD domain involved in transcriptional activation, we performed reporter assays using sHBZ-ΔbZIP and its mutants (Figure 4D top panel). As illustrated in Figure 4D (middle panel), deletion of residues 20 to 38, which contains an LXXLL-like motif (LXXLL1), abrogated the enhancement of TGF-β signaling, whereas removal of the second LXXLL motif (LXXLL2) had no effect. Furthermore, we found that mutation of the LXXLL1 motif resulted in complete loss of activation. Because the LXXLL1 motif of HBZ is the major region where p300 binds,[35] this result further implicates p300 in the activation of TGF-β signaling by HBZ.

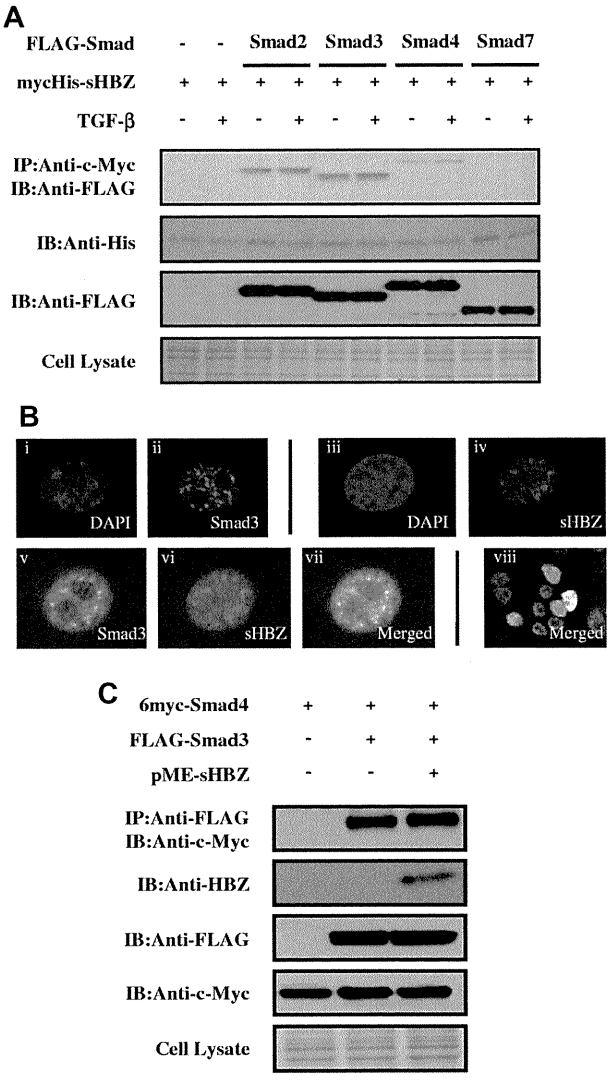

Figure 2. HBZ interacts with Smad proteins. (A) HBZ interacted with Smad proteins. COS7 cells were cotransfected with mycHis-sHBZ (6 μg) and FLAG-Smad2, Smad3, Smad4, and Smad7 (6 μg). At 24 hours after transfection, the cells were treated with or without TGF-β (5 ng/mL). Cell lysates were subjected to immunoprecipitation using anti-c-Myc followed by immunoblotting using anti-FLAG for detection of Smad proteins. (B) sHBZ colocalized with Smad3 in the cell nucleus. COS7 cells were transfected with mycHis-sHBZ (0.6 μg) together with (v-viii) or without (iii-iv) FLAG-Smad3 (0.4 μg). sHBZ was detected using anti-MYC Cy3 antibody (iv,vi). Smad3 was detected using anti–Flag-biotin and secondary streptavidin-Alexa-488 antibody (ii,v). The overlay of sHBZ and Smad3 is shown (vii-viii). DAPI (4,6-diamidino-2-phenylindole) was used to counterstain the nucleus (i,iii). (C) HBZ did not influence the Smad3/Smad4 interaction. COS7 cells were transfected with the indicated expression vectors (3 μg each). Cell lysates were subjected to immunoprecipitation using anti-FLAG followed by immunoblot (IB) using anti–c-Myc.

We mapped the region of HBZ interacting with Smad3 in more detail. As shown in Figure 4E, full-length sHBZ and 2 of its deletion mutants (sHBZ-ΔbZIP and sHBZ-AD+bZIP) associated with Smad3, wheres sHBZ-ΔAD, which lacks the AD domain, has no binding capability. sHBZ-ΔbZIP exhibited higher affinity for Smad3 than did full-length sHBZ. This result corroborates that of the luciferase assay in Figure 4C. To define which part of Smad3 binds HBZ, we performed a coimmunoprecipitation assay with Smad3 mutants in COS7 cells (Figure 4F). We found that Smad3 mutants without MH2 domain could not bind to sHBZ whereas only the MH2 domain of Smad3 physically interacted with sHBZ. Hence, the interaction with HBZ is mediated by the MH2 segment of Smad3 (Figure 4G).

Taken together, these observations demonstrate that HBZ enhances TGF-β signaling by physically associating with Smad3/p300 complexes via its AD domain.

Activation of TGF-β signaling is partially suppressed by high doses of HBZ via inhibition of AP-1

Previous studies have shown that Smads cooperate with AP-1 to mediate TGF-β–induced transcription.[36] In addition, HBZ has been reported to suppress AP-1 activity.[10] The observations shown in Figure 1E and Figure 4C prompted us to ask whether the activated TGF-β signaling was partially suppressed by higher HBZ expression levels because HBZ inhibited AP-1. A reporter assay showed that the suppression of TGF-β-mediated activation by high sHBZ doses (> 200 ng pcDNA3.1-mycHis-sHBZ plasmid DNA per well) was overcome by c-Fos, but not by enforced expression of Smad3, although overexpression of both Smad3 and c-Fos dramatically enhanced HBZ-mediated activation of TGF-β signaling (Figure 5A). To confirm this result, we performed a luciferase assay using a Luc vector, 9 × CAGA-Luc, which contains multiple CAGA sites but lacks AP-1 binding sites. As shown in Figure 5B, sHBZ persistently enhanced TGF-β–mediated activation of this reporter, even at high doses. In addition, we confirmed that the bZIP domain of spliced HBZ is required for the suppression of AP-1 signaling (Figure 5C). This result is consistent with the results of the luciferase assay (Figure 4C), in which sHBZ-ΔbZIP activation of TGF-β signaling was stronger than that of full-length sHBZ. These observations demonstrate that high levels of HBZ expression partially suppress TGF-β signaling by inhibiting AP-1 signaling and that the bZIP domain of HBZ is responsible for this suppressive activity.

Physiologic levels of HBZ overcome Tax-mediated suppression of TGF-β signaling

To rule out the possibility that the activated TGF-β signaling observed in this study was caused by overexpression of HBZ, we compared the expression level of HBZ protein in transfected HepG2 cells with those in ATL- and HTLV-1–associated cell lines. As shown in Figure 6A, HepG2 cells transfected with 200 ng pME18Sneo-sHBZ plasmid DNA per well on 12-well plates expressed sHBZ protein at levels equivalent or slightly higher than those in ATL- and HTLV-1–associated cell lines. This result suggested that sHBZ protein expressed at physiologic levels could therefore activate TGF-β–mediated signaling. Next, we examined the endogenous sHBZ and Smad3 protein complex. The expression of *Smad3* mRNA was variable in fresh ATL cells, ATL cell lines, and HTLV-1–associated cell lines (supplemental Figure 3). sHBZ was detected in the immunoprecipitate pulled down by a specific antibody against Smad3 (Figure 6B). These data further support the interaction between HBZ and Smad3 in HTLV-1–infected cells.

It has been reported that HTLV-1 Tax protein inhibits Smad-dependent TGF-β signaling.[18-20] Next, we performed a reporter assay to study the effect of HBZ on Tax-mediated suppression of TGF-β pathway. When coexpressed with Tax, sHBZ overcame Tax's repression of 3TP luciferase activity. Moreover, Tax had little effect on sHBZ-activated TGF-β signaling when equal amounts of sHBZ and Tax were expressed (Figure 6C).

HBZ enhances Foxp3 expression in naive T cells through Smad3

We next studied the effect of HBZ expression on transcription of TGF-β target genes. We expressed sHBZ in mouse naive T cells using a retrovirus vector. As shown in Figure 7A, expression of

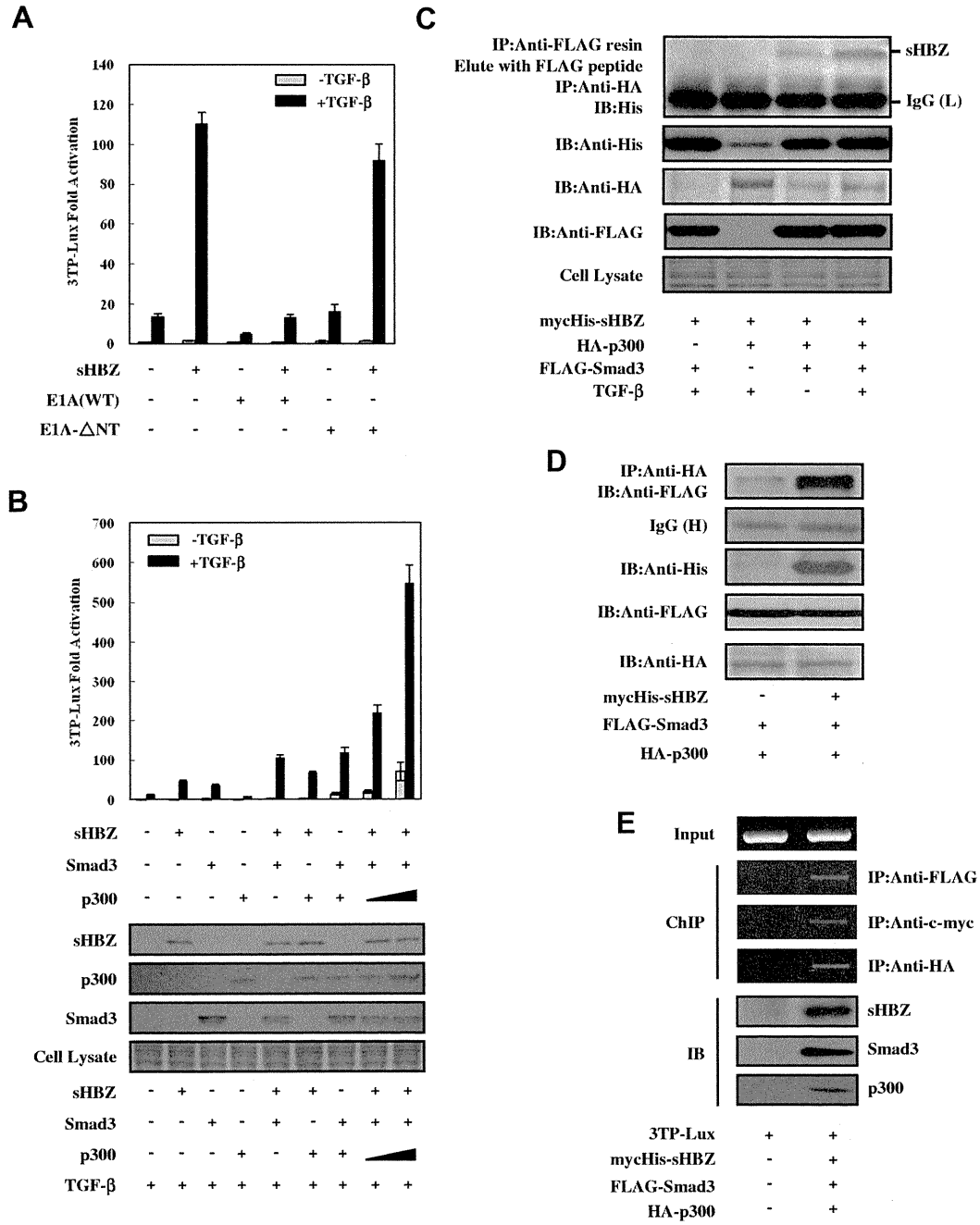

Figure 3. HBZ activates TGF-β signaling dependent on p300. (A) E1A repressed HBZ-induced activation of TGF-β. In 12-well plates, HepG2 cells were cotransfected with 3TP-Lux (0.5 μg), phRL-TK (2 ng), pME18Sneo-sHBZ (20 ng), and pCS2+-E1A or pCS2+-E1A-ΔNT (2 ng). Luciferase activity was measured 24 hours after stimulation by TGF-β (0, 10 ng/mL). (B) HBZ synergized with Smad3 and p300 to enhance TGF-β. HepG2 cells were cotransfected with 3TP-Lux (0.5 μg), phRL-TK (2 ng), pcDNA3.1-mycHis-sHBZ (200 ng), FLAG-Smad3 (50 ng), and pCMV-p300 (2, 5 μg). At 24 hours after transfection, the cells were treated with or without TGF-β (10 ng/mL). Luciferase activity was measured after 24 hours. Expression of sHBZ, Smad3, and p300 was detected by Western blot (middle panel). CBB staining was shown as the loading control (bottom panel). (C) HBZ, Smad3, and p300 could form a ternary complex. mycHis-sHBZ (4 μg), FLAG-Smad3 (4 μg), and HA-p300 (4 μg) were cotransfected into COS7 cells, which were subsequently treated with TGF-β (5 ng/mL). Ternary complexes were detected by sequential immunoprecipitation with anti-FLAG agarose affinity gel and anti-HA antibody, followed by immunoblotting with the His antibody. (D) HBZ enhanced the interaction between Smad3 and p300. COS7 cells were cotransfected with mycHis-sHBZ (4 μg), FLAG-Smad3 (4 μg), and HA-p300 (4 μg). Cell lysates (samples from the experiment of Figure 4E) were subjected to immunoprecipitation using anti-HA followed by immunoblotting with anti-FLAG. (E) sHBZ, Smad3, and p300 bind to the Smad-responsive promoter. After transfection with mycHis-sHBZ, FLAG-Smad3, and HA-p300, and treatment with 5 ng/mL of TGF-β for 24 hours, HepG2 cells were chromatin immunoprecipitated by each indicated antibody. The precipitated DNAs and 1% of the input cell lysates were amplified by the 3TP promoter specific primers. Expression of sHBZ, Smad3, and p300 was detected by Western blot (bottom panel).

sHBZ was associated with enhanced transcription of *Pdgfb*, *Sox4*, *Ctgf*, *Foxp3*, *Runx1*, and *Tsc22d1* genes and suppression of *Id2* gene; such effects were consistent with those by TGF-β. However, HBZ did not influence the level of *Cdkn1a*, *Cdkn2b*, and *Myc* gene transcripts. This result indicates that HBZ selectively modulates transcription of TGF-β target genes, such as TGF-β. HBZ does not interfere with the expression of genes associated with cell cycle and proliferation. To check whether HBZ could affect the cell growth via enhancing TGF-β signaling, we established stable sHBZ-expressing CTLL-2 cell lines. TGF-β suppressed proliferation of

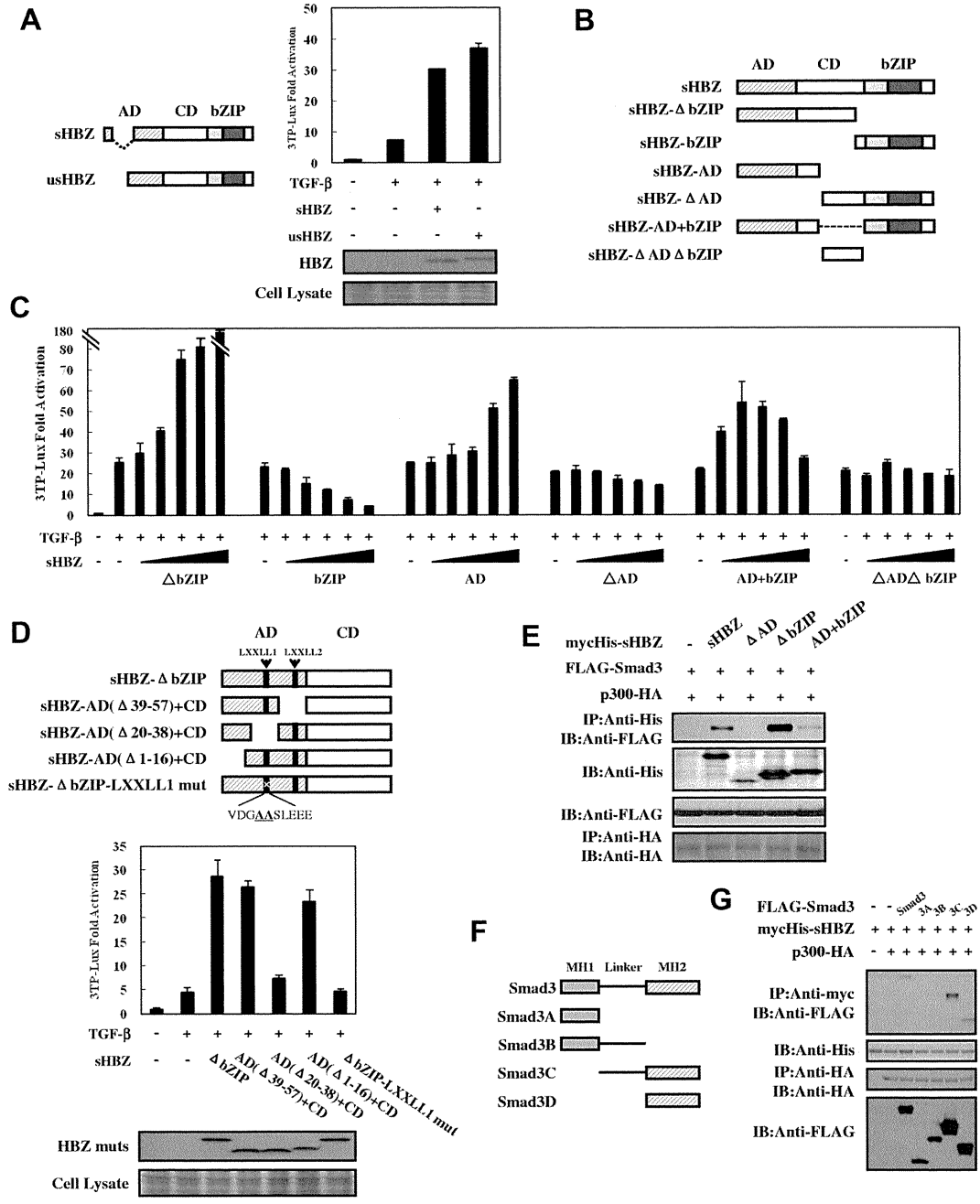

Figure 4. Domains of HBZ responsible for the activation of TGF-β signaling. (A) Comparison of the effect of sHBZ and usHBZ on TGF-β activation. (Left panel) Schematic diagram of sHBZ and usHBZ. (Right panel) HepG2 cells were cotransfected with 3TP-Lux (0.5 μg), phRL-TK (2 ng), pcDNA3.1-mycHis-sHBZ, or pcDNA3.1-mycHis-usHBZ (200 ng). Luciferase activity was measured 24 hours after 10 ng/mL TGF-β stimulation. mycHis tagged sHBZ and usHBZ were detected by Western blot (middle panel). CBB staining was shown as the loading control (bottom panel). (B) Schematic diagram of sHBZ and its mutants used in this study. Characteristic domains of sHBZ are indicated as follows: AD, CD, and basic leucine zipper domain (bZIP). (C) Analysis of sHBZ deletion mutants for their effect on TGF-β–mediated signaling. In 12-well plates, HepG2 cells were cotransfected with 3TP-Lux (0.5 μg), phRL-TK (2 ng), and pME18Sneo-sHBZ mutants (0, 5, 20, 100, 200, and 500 ng). Luciferase activity was measured 24 hours after stimulation by TGF-β (10 ng/mL). (D) The N-terminal LXXLL1 motif of HBZ is important in enhancing TGF-β–induced luciferase expression. (Top panel) Schema of sHBZ-ΔbZIP and its deletion mutants. The locations of the LXXLL motifs are indicated. The mutated residues in the LXXLL1 motif are in bold and underlined. (Middle panel) In 24-well plates, HepG2 cells were cotransfected with 3TP-Lux (0.25 μg), phRL-TK (1 ng), and mycHis-sHBZ-ΔbZIP or its mutants (1 μg). At 24 hours after transfection, the cells were stimulated with or without 10 ng/mL TGF-β. Cell lysates were subjected to luciferase assay 24 hours after stimulation. sHBZ-ΔbZIP and its mutants were detected by Western blot. CBB staining was shown as the loading control (bottom panel). (E) Determination of the region of HBZ responsible for the interaction with Smad3. COS7 cells were transfected with the indicated mycHis-sHBZ mutants along with the FLAG-Smad3 and HA-p300 vectors. Cell lysates were subjected to immunoprecipitation using anti–c-Myc followed by immunoblotting using anti-FLAG. (F) Schematic drawing of Smad3 and its deletion mutants. The locations of the MH1 domain, MH2 domain, and the linker domain are indicated. (G) Mapping the region of the Smad3 protein necessary for interaction with sHBZ. COS7 cells were transfected with HA-p300, mycHis-sHBZ, and full-length or mutant FLAG-Smad3. At 48 hours after transfection, total cell lysates were subjected to immunoprecipitation using anti–c-Myc followed by IB using anti-FLAG.

control CTLL-2 cells, whereas HBZ expressing CTLL-2 cells proliferated regardless of TGF-β (Figure 7B).

It has been reported that TGF-β signaling is critical for the development of $CD4^+CD25^+Foxp3^+$ regulatory T cells and that the binding of Smad3 to a specific enhancer region is required for activation of the *Foxp3* promoter.[21,29] As shown in Figure 7A, HBZ enhanced transcription of *Foxp3* gene induced by TGF-β. We therefore studied whether HBZ has any influence on the generation

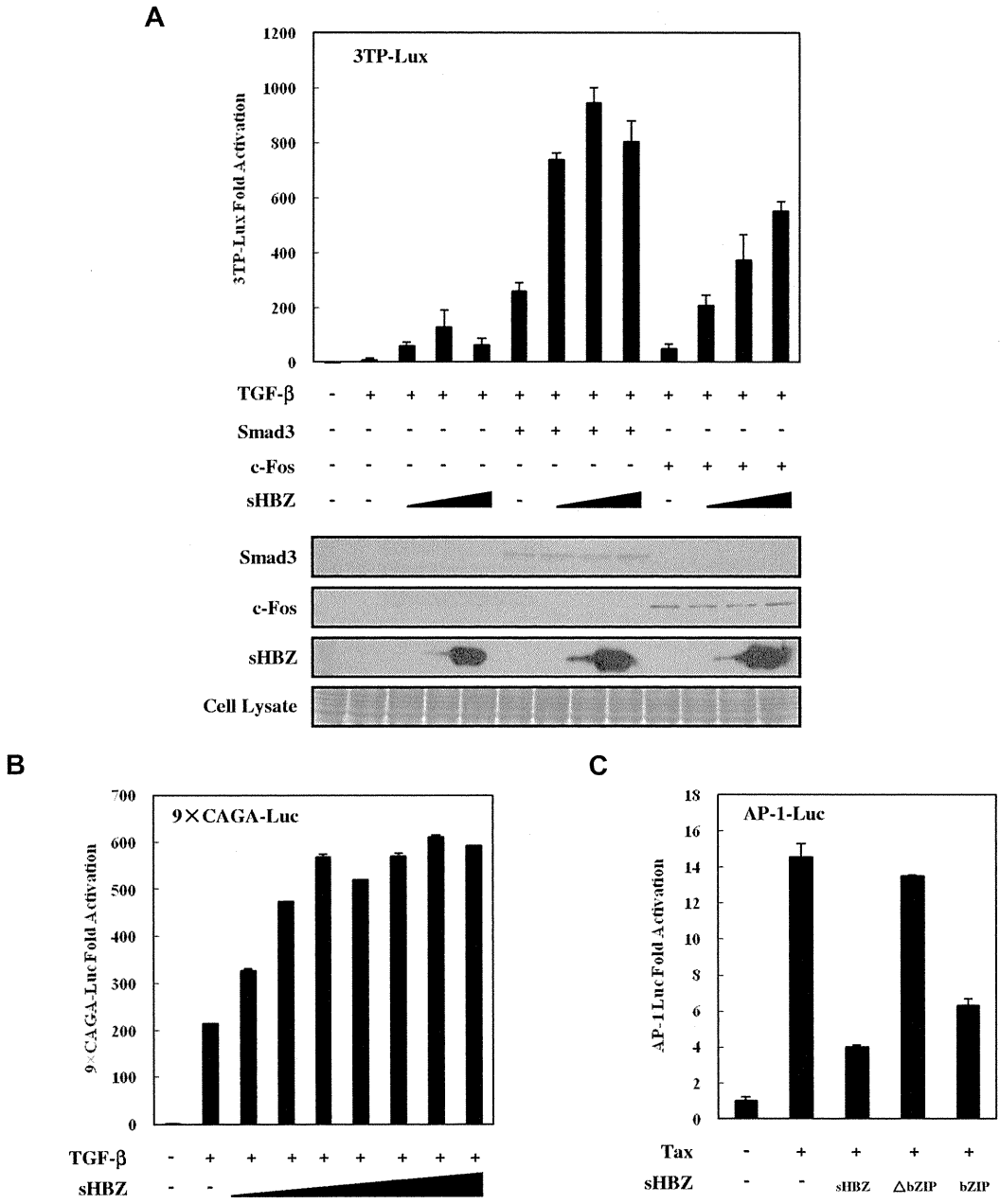

Figure 5. Higher expression of HBZ partially suppressed activation of TGF-β signaling via AP-1. (A) HepG2 cells were cotransfected with 3TP-Lux (0.5 μg), phRL-TK (2 ng), pCDNA3-c-Fos (0, 0.1 μg), FLAG-Smad3 (0, 0.1 μg), and pcDNA3.1-mycHis-sHBZ (0, 20, 200, and 4000 ng). At 24 hours after transfection, the cells were treated with or without TGF-β (10 ng/mL). After 24 hours, the cells were harvested, and luciferase activity was determined. Expression of sHBZ, Smad3, and c-Fos was detected by Western blot (middle panel). CBB staining was shown as the loading control (bottom panel). (B) HepG2 cells were cotransfected with 9 × CAGA-Luc (0.5 μg), phRL-TK (2 ng), and pME18Sneo-sHBZ (0, 2, 5, 10, 20, 50, 100, and 200 ng). Luciferase activity was measured 24 hours after 10 ng/mL TGF-β stimulation. (C) sHBZ inhibited AP-1 signaling via its bZIP domain. Jurkat cells were cotransfected with AP-1-Luc (1 μg), phRL-TK (10 ng), pCG-Tax (1 μg), and pME18Sneo-sHBZ mutants (1 μg). After 48 hours, luciferase activity was measured.

of Foxp3$^+$ T cells. Retrovirally expressed sHBZ protein increased the level of Foxp3 in conventional mouse CD4$^+$ T cells and also synergistically enhanced TGF-β–induced Foxp3 expression (Figure 7C,E). Treatment with SB431542, an inhibitor of the TGF-β type I receptor, did not change the induction of Foxp3 by sHBZ, whereas it completely blocked the TGF-β–induced Foxp3 expression (Figure 7C), indicating that an increase in TGF-β cytokine was not involved in this synergistic effect. sHBZ also induced FoxP3 expression in human naive T cells (Figure 7D).

Apart from Smad3, STAT5 is the main factor that sustains Foxp3 expression in both Treg and effector T cells.[37] Therefore, we next evaluated the effect of HBZ on STAT5 signaling. sHBZ was not capable of activating CA-STAT5a-mediated transcriptional activation of the Jγ1 promoter (supplemental Figure 4). Therefore, it is probable that HBZ induced the expression of Foxp3 through TGF-β/Smad3 responses. After treatment with SIS3, a specific inhibitor of Smad3, sHBZ-enhanced Foxp3 induction was reduced by > 70% (Figure 7E). Furthermore, the synergistic effect of sHBZ on TGF-β–induced Foxp3 expression was markedly inhibited by SIS3 (Figure 7E).

To further analyze the mechanism by which HBZ induces Foxp3 expression, we performed a reporter assay using the

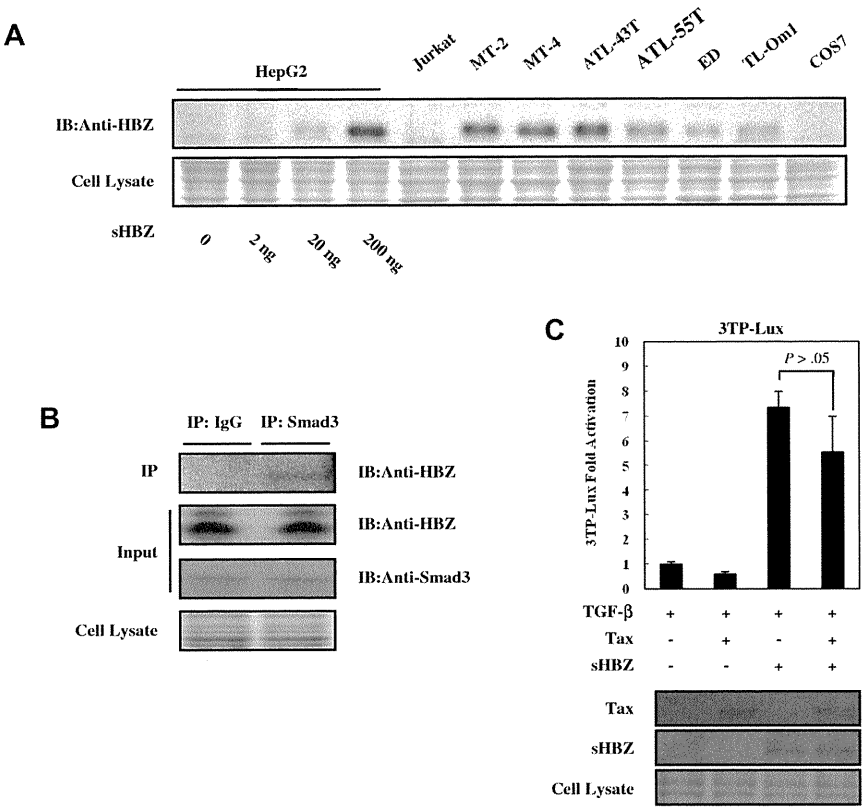

Figure 6. Physiologic level of HBZ overcame the Tax-mediated suppression of TGF-β signaling. (A) Comparing the level of HBZ protein in HBZ-transfected HepG2 cells with the level of HBZ in ATL and HTLV-1–immortalized cell lines. Total protein was extracted from sHBZ-transfected HepG2 cells (samples from supplemental Figure 1) and the indicated cell lines, and subjected to immunoblotting using HBZ antibody. (B) Endogenous HBZ interacted with Smad3. ATL-55T cells were treated with 10 ng/mL TGF-β. After 10 hours, whole cell lysate was subjected to immunoprecipitation with anti-Smad3 or control IgG, and immunoprecipitates were probed with anti-HBZ antibody. (C) HBZ overcame the repression of TGF-β signaling induced by Tax. In 12-well plates, HepG2 cells were cotransfected with 3TP-Lux (0.5 μg), phRL-TK (2 ng), pCG-Tax (0, 0.2 μg), and pcDNA3.1-mycHis-sHBZ (0, 0.2 μg). At 24 hours after transfection, the cells were treated with or without 10 ng/mL TGF-β. After 24 hours, the cells were harvested and analyzed for luciferase activity. sHBZ and Tax were detected by Western blot (middle panel). CBB staining was shown as the loading control (bottom panel).

enhancer and promoter of the mouse *Foxp3* gene. As shown in Figure 7F, sHBZ activated Foxp3-Luciferase expression but it failed to activate the *Foxp3* promoter alone, indicating that the *Foxp3* gene is regulated by HBZ through the enhancer. We next examined the contribution of Smad3 to HBZ-induced *Foxp3* enhancer activity. *Foxp3* reporter activity was reduced after mutation of the Smad-binding region of the enhancer, and treatment with SIS3 completely blocked the transactivation of *Foxp3* by sHBZ (Figure 7F). Furthermore, interaction of HBZ, Smad3, and p300 to human *FoxP3* enhancer was detected by ChIP assay in a HTLV-1–transformed cell line, MT-2 (Figure 7G). These results collectively indicate that the enhanced induction of Foxp3 expression by HBZ can be attributed, at least in part, to Smad3-dependent TGF-β signaling.

Discussion

Leukemic cells in most ATL cases, like Tregs, express CD4, and CD25. Foxp3 is a master regulator that controls the transcription of genes, which are critical for the suppressive function of Tregs. Two-thirds of ATL cases express FoxP3 in the tumor cells, indicating that such ATL cells are derived from Tregs.[23] Indeed, it has been reported that ATL cells have a suppressive effect on bystander $CD4^+$ T cells.[38] The proportion of HTLV-1 provirus is higher in $FoxP3^+$ Tregs than in uninfected cells.[24] Thus, these findings suggest that HTLV-1 infection increases virus-infected Tregs and finally transforms them. So far, the molecular mechanisms underlying the development of ATL Tregs have not been defined. TGF-β signaling has been implicated in both the development and function of Tregs,[21] and recently we reported that transgenic expression of the *HBZ* gene increased Tregs in vivo and HBZ enhanced transcription of the *Foxp3* gene.[26] Thus, HBZ induces Foxp3 expression and promotes Treg cell development in vivo. The present study links HBZ and TGF-β signaling by showing that HBZ induces Foxp3 expression via interaction with Smad3 and p300. Although HBZ impairs the suppressive function of Tregs to some extent, HBZ-expressing Tregs retain some suppressive functions.[26] Indeed, the immunodeficiency observed in ATL patients and HTLV-1 carriers might be attributable to the Treg phenotype induced by HBZ. The weak immunosuppressive potential retained by HTLV-1–infected Tregs may allow them to escape host immune attack, which possibly explains why HTLV-1 favors Tregs in vivo.

Several viruses have evolved distinct strategies to modulate TGF-β signaling using their own viral proteins. Examples include hepatitis B virus pX; hepatitis C virus core protein, NS3 and NS5; Kaposi sarcoma-associated herpesvirus K-bZIP; Epstein-Barr virus LMP1; and severe acute respiratory syndrome-associated coronavirus N protein.[39-44] Like HBZ, the HBV pX and severe acute respiratory syndrome N protein enhance the transcriptional responses of TGF-β. The common strategy used by viruses to modulate TGF-β signaling is the direct binding of viral proteins to Smad proteins. In this study, we demonstrated that the enhancement of the p300/Smad3 interaction by HBZ is critical for HBZ-induced TGF-β activation.

TGF-β exerts growth inhibitory effects, from which cancer cells usually escape during malignant progression. Accumulating evidence shows that TGF-β act as tumor suppressor at early stages of cancer development but can promote tumor progression at later stages of oncogenesis through tumor-cell-autonomous and host-tumor interactions. Like other cancer cells, HTLV-1–infected T cells are resistant to the growth-inhibitory effect of TGF-β.[45] As a mechanism of this resistance, Tax has been shown to inhibit TGF-β–mediated signaling, resulting in escape from the suppressive effect of TGF-β.[18-20] It is possible that Tax protein inhibits the

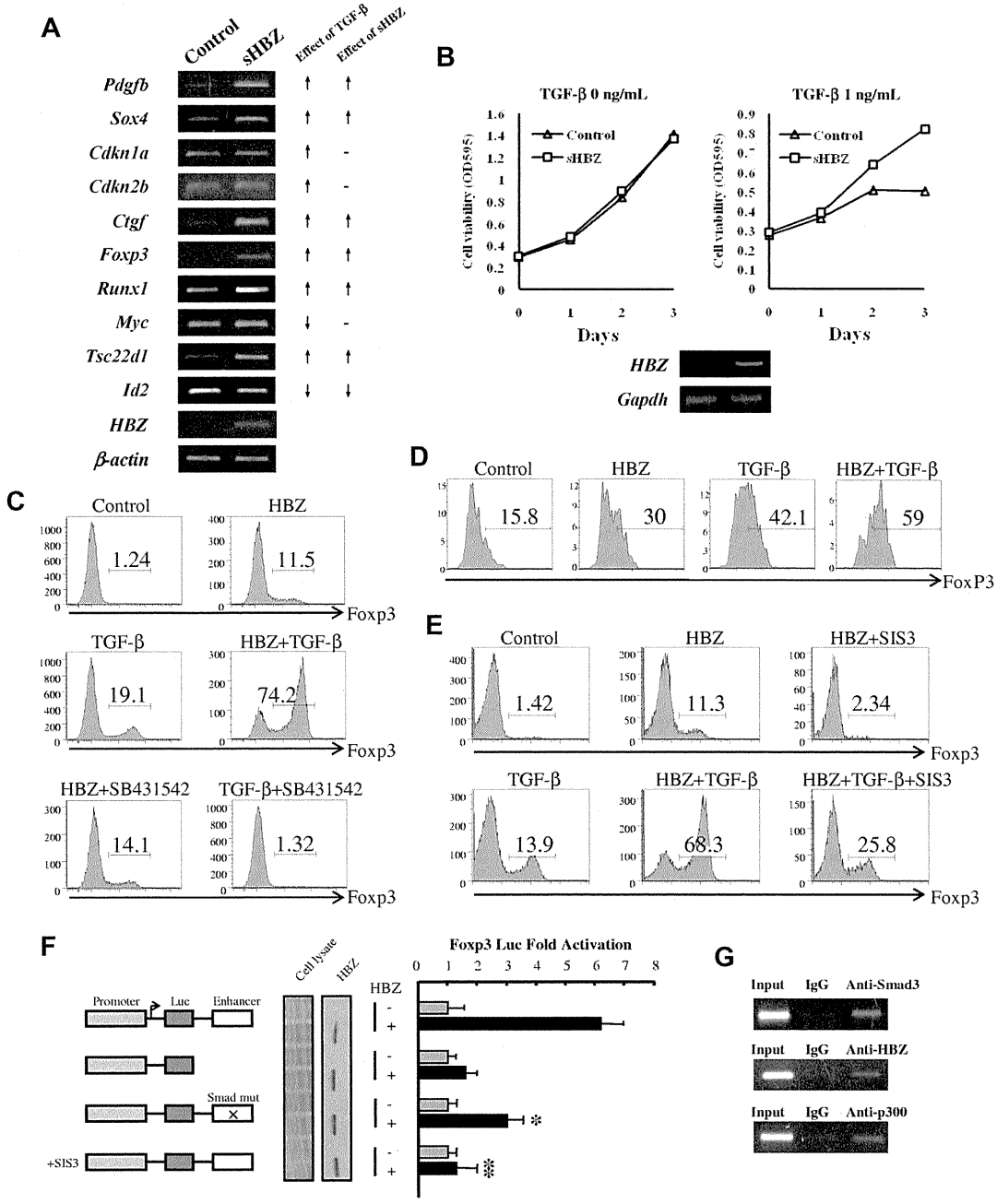

Figure 7. HBZ induced Foxp3 expression in naive T cells through Smad3. (A) HBZ modulated the expression of selected TGF-β target genes. (Left panel) Mouse naive T cells were transduced with pMXs-IG vector encoding sHBZ or empty vector. Forty-eight hours after viral infection, total RNA was extracted from sorted green fluorescent protein-positive cells. The level of *Pdgfb*, *Sox4*, *Cdkn1a*, *Cdkn2b*, *Ctgf*, *Foxp3*, *Runx1*, *Myc*, *Tsc22d1*, *Id2*, β-*actin*, and *HBZ* mRNA was analyzed by semiquantitative RT-PCR. (Right panel) Schema of the effect of TGF-β and sHBZ on TGF-β target gene transcription. ↑ indicates up-regulation; ↓, down-regulation; and -, no effect. (B) CTLL-2/pME18Sneo and CTLL-2/sHBZ, cells were plated in 96-well plates. Cells were treated with increasing concentrations of TGF-β for 72 hours. Proliferation of each cell was examined by methyl thiazolyl tetrazolium assay. Expression of *HBZ* was detected by RT-PCR (bottom panel). (C) SB431542, an inhibitor of the TGF-β receptor, could not inhibit the induction of Foxp3 by HBZ. Mouse $CD4^+CD25^-$ T cells were transduced with pGCDNsaml/N vector encoding sHBZ, or with empty vector. Three days after TGF-β (0.2 ng/mL) and SB431542 (5μM) treatment, cells were stained with anti-Foxp3 in addition to anti-NGFR and then analyzed by flow cytometry. Numbers indicate the percentage of Foxp3-positive cells among NGFR-positive cells. (D) HBZ induced FoxP3 in human naive T cells. Human $CD4^+CD25^-$ T cells were transfected with lentiviral vectors expressing sHBZ, or with empty vector. Two days after stimulating with TGF-β (0.1 ng/mL), cells were stained with antibodies for CD4, NGFR, and Foxp3 and then analyzed by flow cytometry. (E) SIS3 inhibited the HBZ-induced Foxp3 induction. Mouse $CD4^+CD25^-$ T cells were transduced with pGCDNsaml/N vector encoding sHBZ or empty vector. Fifteen hours after viral infection, SIS3 (5μM) and TGF-β (1 ng/mL) were added. Thirty-six hours after treatment, Foxp3 expression was detected by flow cytometry. Numbers indicate the percentage of Foxp3-positive cells among NGFR-positive cells. Representative data from 3 independent experiments are shown. (F) HBZ activated transcription of the *Foxp3* promoter through its Smad site of enhancer. EL4 cells were transfected with the Foxp3 reporter plasmid or its mutants with or without the sHBZ-expressing plasmid (pcDNA3.1-mycHis-sHBZ). Luciferase activity was measured 48 hours after stimulation by TGF-β. Expression of sHBZ was detected by Western blot. CBB staining was shown as the loading control. (G) HBZ formed complex with Smad3/p300 in *FoxP3* enhancer. MT-2 cells treated with 5 ng/mL of TGF-β for 2 hours, and chromatin immunoprecipitated by each indicated antibody. The precipitated DNAs and 1% of the input cell lysates were amplified by the specific primers for *FoxP3* enhancer.

growth suppressive effect of TGF-β in the early stage of ATL, whereas other mechanisms, which include increased expression of Smad7,[46] and aberrant expression of MEL1S,[27] suppress cytostatic effects of TGF-β/Smad signaling pathway when Tax expression is lost in the late stage. However, as shown in this study, HBZ-expressing CTLL-2 cells could proliferate in the presence of

TGF-β. There are 2 possible scenarios. HBZ selectively modulates actions of TGF-β/Smad signaling pathway as shown in this study, which possibly does not influence transcription of TGF-β target genes associated with cell cycle and proliferation. Alternatively, because HBZ has growth-promoting activity,[7] it might counteract cytostatic activity of TGF-β, whereas other activities of TGF-β/Smad signaling pathway are enhanced by HBZ. It has been reported that tumors use the TGF-β/Smad system to induce gene responses that promote tumor growth, invasion, evasion of immune surveillance, and metastasis.[47] In HTLV-1, an important function of activated TGF-β/Smad pathway by HBZ is up-regulation of the *Foxp3* gene transcription and induction of Tregs. Further studies on TGF-β signaling in ATL are necessary to clarify its roles.

Dysregulation of TGF-β signaling has been reported in HTLV-1–associated HAM/TSP.[48] Expressions of TGF-β receptor II and Smad7 were suppressed in T cells of HAM/TSP patients, suggesting that these abnormalities are implicated in perturbed immune tolerance. As shown in Figure 6C, activation of TGF-β signaling by HBZ is more predominant than the suppressive effect by Tax, which might account for why more than half of ATL cases express FoxP3,[23] and the proportion of FoxP3$^+$ Tregs is higher in Tax$^+$ T cells derived from HTLV-1 carriers and HAM/TSP patients.[24] However, Smad7 expression is increased in ATL cells, indicating that TGF-β signaling is different between leukemic and carrier state. To elucidate the entire picture of TGF-β signaling in HTLV-1 infection and ATL needs further studies.

It has been reported that HBZ suppresses viral transcription from the HTLV-1 long terminal repeat by disturbing the interaction between Tax and p300/CBP, thereby displacing p300 from the viral promoter.[35] However, our report showed that the binding of HBZ with p300 stabilized the Smad3-p300 complex, resulting in TGF-β activation. HBZ competes with Tax for the same domain of p300, whereas HBZ and Smad3 have different p300 binding sites. We speculate that HBZ activation or repression of p300 transcriptional activation is dependent on the p300 binding partner. It is also probable that the function of the HBZ-p300 complex depends on the capacity of HBZ to recruit p300 onto the DNA element, a bimodal effect similar to that previously reported for the Tax-p300/CBP complex.[49] Consistent with our findings, a recent study reported that HBZ activated transcription of *DKK1* gene by interacting with the cellular coactivators p300 and CBP.[50]

In conclusion, we showed that HBZ enhanced TGF-β signaling by physically interacting with Smad3/p300, leading to the up-regulation of TGF-β target genes, including *Foxp3*. HTLV-1 may take advantage of this mechanism to elude host immune attack, allowing the infected cells to proliferate in vivo.

Acknowledgments

This work was supported by the Ministry of Education, Science, Sports, and Culture of Japan (Scientific Research Grant-in-aid), the Novartis Foundation (M.M.), and the National Institutes of Health (CA77556 and CA100730, P.L.G.).

Authorship

Contribution: T.Z., Y.S., T.I., and M.M. designed the research; T.Z., Y.S., K.S., and P.M. performed the research; P.L.G. and T.I. provided vital reagents; T.Z., Y.S., and M.M. analyzed the data; and T.Z., Y.S., P.L.G., T.I., and M.M. wrote the paper.

Conflict-of-interest disclosure: The authors declare no competing financial interests.

Correspondence: Masao Matsuoka, Laboratory of Virus Control, Institute for Virus Research, Kyoto University, 53 Shogoin Kawahara-cho, Sakyo-ku, Kyoto 606-8507, Japan; e-mail: mmatsuok@virus.kyoto-u.ac.jp.

References

1. Uchiyama T, Yodoi J, Sagawa K, Takatsuki K, Uchino H. Adult T-cell leukemia: clinical and hematologic features of 16 cases. *Blood.* 1977; 50(3):481-492.
2. Poiesz BJ, Ruscetti FW, Gazdar AF, Bunn PA, Minna JD, Gallo RC. Detection and isolation of type C retrovirus particles from fresh and cultured lymphocytes of a patient with cutaneous T-cell lymphoma. *Proc Natl Acad Sci U S A.* 1980; 77(12):7415-7419.
3. Nicot C, Harrod RL, Ciminale V, Franchini G. Human T-cell leukemia/lymphoma virus type 1 nonstructural genes and their functions. *Oncogene.* 2005;24(39):6026-6034.
4. Grassmann R, Aboud M, Jeang KT. Molecular mechanisms of cellular transformation by HTLV-1 Tax. *Oncogene.* 2005;24(39):5976-5985.
5. Matsuoka M, Jeang KT. Human T-cell leukaemia virus type 1 (HTLV-1) infectivity and cellular transformation. *Nat Rev Cancer.* 2007;7(4):270-280.
6. Gaudray G, Gachon F, Basbous J, Biard-Piechaczyk M, Devaux C, Mesnard JM. The complementary strand of the human T-cell leukemia virus type 1 RNA genome encodes a bZIP transcription factor that down-regulates viral transcription. *J Virol.* 2002;76(24):12813-12822.
7. Satou Y, Yasunaga J, Yoshida M, Matsuoka M. HTLV-I basic leucine zipper factor gene mRNA supports proliferation of adult T cell leukemia cells. *Proc Natl Acad Sci U S A.* 2006;103(3):720-725.
8. Basbous J, Arpin C, Gaudray G, Piechaczyk M, Devaux C, Mesnard JM. The HBZ factor of human T-cell leukemia virus type I dimerizes with transcription factors JunB and c-Jun and modulates their transcriptional activity. *J Biol Chem.* 2003;278(44):43620-43627.
9. Lemasson I, Lewis MR, Polakowski N, et al. Human T-cell leukemia virus type 1 (HTLV-1) bZIP protein interacts with the cellular transcription factor CREB to inhibit HTLV-1 transcription. *J Virol.* 2007;81(4):1543-1553.
10. Matsumoto J, Ohshima T, Isono O, Shimotohno K. HTLV-1 HBZ suppresses AP-1 activity by impairing both the DNA-binding ability and the stability of c-Jun protein. *Oncogene.* 2005;24(6):1001-1010.
11. Zhao T, Yasunaga J, Satou Y, et al. Human T-cell leukemia virus type 1 bZIP factor selectively suppresses the classical pathway of NF-kappaB. *Blood.* 2009;113(12):2755-2764.
12. Fan J, Ma G, Nosaka K, et al. APOBEC3G generates nonsense mutations in HTLV-1 proviral genomes in vivo. *J Virol.* 2010;84(14):7278-7287.
13. Massague J, Blain SW, Lo RS. TGFbeta signaling in growth control, cancer, and heritable disorders. *Cell.* 2000;103(2):295-309.
14. Janknecht R, Wells NJ, Hunter T. TGF-beta-stimulated cooperation of smad proteins with the coactivators CBP/p300. *Genes Dev.* 1998;12(14): 2114-2119.
15. Feng XH, Derynck R. Specificity and versatility in TGF-β signaling through Smads. *Annu Rev Cell Dev Biol.* 2005;21:659-693.
16. Kim SJ, Kehrl JH, Burton J, et al. Transactivation of the transforming growth factor beta 1 (TGF-beta 1) gene by human T lymphotropic virus type 1 tax: a potential mechanism for the increased production of TGF-beta 1 in adult T cell leukemia. *J Exp Med.* 1990;172(1):121-129.
17. Niitsu Y, Urushizaki Y, Koshida Y, et al. Expression of TGF-beta gene in adult T cell leukemia. *Blood.* 1988;71(1):263-266.
18. Arnulf B, Villemain A, Nicot C, et al. Human T-cell lymphotropic virus oncoprotein Tax represses TGF-beta 1 signaling in human T cells via c-Jun activation: a potential mechanism of HTLV-I leukemogenesis. *Blood.* 2002;100(12):4129-4138.
19. Lee DK, Kim BC, Brady JN, Jeang KT, Kim SJ. Human T-cell lymphotropic virus type 1 tax inhibits transforming growth factor-beta signaling by blocking the association of Smad proteins with Smad-binding element. *J Biol Chem.* 2002; 277(37):33766-33775.
20. Mori N, Morishita M, Tsukazaki T, et al. Human T-cell leukemia virus type I oncoprotein Tax represses Smad-dependent transforming growth factor beta signaling through interaction with CREB-binding protein/p300. *Blood.* 2001;97(7): 2137-2144.
21. Bommireddy R, Doetschman T. TGFbeta1 and Tregs: alliance for tolerance. *Trends Mol Med.* 2007;13(11):492-501.
22. Hori S, Sakaguchi S. Foxp3: a critical regulator of the development and function of regulatory T cells. *Microbes Infect.* 2004;6(8):745-751.
23. Karube K, Ohshima K, Tsuchiya T, et al. Expression of FoxP3, a key molecule in CD4CD25 regulatory T cells, in adult T-cell leukaemia/lymphoma cells. *Br J Haematol.* 2004;126(1):81-84.

24. Toulza F, Heaps A, Tanaka Y, Taylor GP, Bangham CR. High frequency of CD4+FoxP3+ cells in HTLV-1 infection: inverse correlation with HTLV-1-specific CTL response. *Blood.* 2008; 111(10):5047-5053.
25. Yamano Y, Takenouchi N, Li HC, et al. Virus-induced dysfunction of CD4+CD25+ T cells in patients with HTLV-I-associated neuroimmunological disease. *J Clin Invest.* 2005;115(5):1361-1368.
26. Satou Y, Yasunaga J, Zhao T, et al. HTLV-1 bZIP factor induces T-cell lymphoma and systemic inflammation in vivo. *PLoS Pathog.* 2011;7(2): e1001274.
27. Yoshida M, Nosaka K, Yasunaga J, Nishikata I, Morishita K, Matsuoka M. Aberrant expression of the MEL1S gene identified in association with hypomethylation in adult T-cell leukemia cells. *Blood.* 2004;103(7):2753-2760.
28. Kahata K, Hayashi M, Asaka M, et al. Regulation of transforming growth factor-beta and bone morphogenetic protein signalling by transcriptional coactivator GCN5. *Genes Cells.* 2004;9(2):143-151.
29. Tone Y, Furuuchi K, Kojima Y, Tykocinski ML, Greene MI, Tone M. Smad3 and NFAT cooperate to induce Foxp3 expression through its enhancer. *Nat Immunol.* 2008;9(2):194-202.
30. Arnold J, Yamamoto B, Li M, et al. Enhancement of infectivity and persistence in vivo by HBZ, a natural antisense coded protein of HTLV-1. *Blood.* 2006;107(10):3976-3982.
31. Arnold J, Zimmerman B, Li M, Lairmore MD, Green PL. Human T-cell leukemia virus type-1 antisense-encoded gene, Hbz, promotes T-lymphocyte proliferation. *Blood.* 2008;112(9): 3788-3797.
32. Morita S, Kojima T, Kitamura T. Plat-E: an efficient and stable system for transient packaging of retroviruses. *Gene Ther.* 2000;7(12):1063-1066.
33. Miyagishi M, Fujii R, Hatta M, et al. Regulation of Lef-mediated transcription and p53-dependent pathway by associating beta-catenin with CBP/p300. *J Biol Chem.* 2000;275(45):35170-35175.
34. Akiyoshi S, Inoue H, Hanai J, et al. c-Ski acts as a transcriptional co-repressor in transforming growth factor-beta signaling through interaction with smads. *J Biol Chem.* 1999;274(49):35269-35277.
35. Clerc I, Polakowski N, Andre-Arpin C, et al. An interaction between the human T cell leukemia virus type 1 basic leucine zipper factor (HBZ) and the KIX domain of p300/CBP contributes to the down-regulation of tax-dependent viral transcription by HBZ. *J Biol Chem.* 2008;283(35):23903-23913.
36. Zhang Y, Feng XH, Derynck R. Smad3 and Smad4 cooperate with c-Jun/c-Fos to mediate TGF-beta-induced transcription. *Nature.* 1998; 394(6696):909-913.
37. Passerini L, Allan SE, Battaglia M, et al. STAT5-signaling cytokines regulate the expression of FOXP3 in CD4+CD25+ regulatory T cells and CD4+CD25- effector T cells. *Int Immunol.* 2008; 20(3):421-431.
38. Chen S, Ishii N, Ine S, et al. Regulatory T cell-like activity of Foxp3+ adult T cell leukemia cells. *Int Immunol.* 2006;18(2):269-277.
39. Cheng PL, Chang MH, Chao CH, Lee YH. Hepatitis C viral proteins interact with Smad3 and differentially regulate TGF-beta/Smad3-mediated transcriptional activation. *Oncogene.* 2004; 23(47):7821-7838.
40. Choi SH, Hwang SB. Modulation of the transforming growth factor-beta signal transduction pathway by hepatitis C virus nonstructural 5A protein. *J Biol Chem.* 2006;281(11):7468-7478.
41. Lee DK, Park SH, Yi Y, et al. The hepatitis B virus encoded oncoprotein pX amplifies TGF-beta family signaling through direct interaction with Smad4: potential mechanism of hepatitis B virus-induced liver fibrosis. *Genes Dev.* 2001;15(4): 455-466.
42. Prokova V, Mosialos G, Kardassis D. Inhibition of transforming growth factor beta signaling and Smad-dependent activation of transcription by the Latent Membrane Protein 1 of Epstein-Barr virus. *J Biol Chem.* 2002;277(11):9342-9350.
43. Tomita M, Choe J, Tsukazaki T, Mori N. The Kaposi's sarcoma-associated herpesvirus K-bZIP protein represses transforming growth factor beta signaling through interaction with CREB-binding protein. *Oncogene.* 2004;23(50):8272-8281.
44. Zhao X, Nicholls JM, Chen YG. Severe acute respiratory syndrome-associated coronavirus nucleocapsid protein interacts with Smad3 and modulates transforming growth factor-beta signaling. *J Biol Chem.* 2008;283(6):3272-3280.
45. Hollsberg P, Ausubel LJ, Hafler DA. Human T cell lymphotropic virus type I-induced T cell activation: resistance to TGF-beta 1-induced suppression. *J Immunol.* 1994;153(2):566-573.
46. Nakahata S, Yamazaki S, Nakauchi H, Morishita K. Downregulation of ZEB1 and overexpression of Smad7 contribute to resistance to TGF-beta1-mediated growth suppression in adult T-cell leukemia/lymphoma. *Oncogene.* 2010;29(29): 4157-4169.
47. Bierie B, Moses HL. Tumour microenvironment: TGFbeta: the molecular Jekyll and Hyde of cancer. *Nat Rev Cancer.* 2006;6(7):506-520.
48. Grant C, Oh U, Yao K, Yamano Y, Jacobson S. Dysregulation of TGF-beta signaling and regulatory and effector T-cell function in virus-induced neuroinflammatory disease. *Blood.* 2008;111(12): 5601-5609.
49. Suzuki T, Uchida-Toita M, Yoshida M. Tax protein of HTLV-1 inhibits CBP/p300-mediated transcription by interfering with recruitment of CBP/p300 onto DNA element of E-box or p53 binding site. *Oncogene.* 1999;18(28):4137-4143.
50. Polakowski N, Gregory H, Mesnard JM, Lemasson I. Expression of a protein involved in bone resorption, Dkk1, is activated by HTLV-1 bZIP factor through its activation domain. *Retrovirology.* 2010;7:61.

Bioorganic & Medicinal Chemistry 19 (2011) 6735–6742

Contents lists available at SciVerse ScienceDirect

Bioorganic & Medicinal Chemistry

journal homepage: www.elsevier.com/locate/bmc

Small molecular CD4 mimics as HIV entry inhibitors

Tetsuo Narumi [a], Hiroshi Arai [a], Kazuhisa Yoshimura [b], Shigeyoshi Harada [b], Wataru Nomura [a], Shuzo Matsushita [b], Hirokazu Tamamura [a,*]

[a] Institute of Biomaterials and Bioengineering, Tokyo Medical and Dental University, Chiyoda-ku, Tokyo 101-0062, Japan
[b] Center for AIDS Research, Kumamoto University, Kumamoto 860-0811, Japan

ARTICLE INFO

Article history:
Received 5 August 2011
Revised 23 September 2011
Accepted 24 September 2011
Available online 29 September 2011

Keywords:
CD4 mimic
HIV entry
gp120-CD4 interaction
Phe43 cavity

ABSTRACT

Derivatives of CD4 mimics were designed and synthesized to interact with the conserved residues of the Phe43 cavity in gp120 to investigate their anti-HIV activity, cytotoxicity, and CD4 mimicry effects on conformational changes of gp120. Significant potency gains were made by installation of bulky hydrophobic groups into the piperidine moiety, resulting in discovery of a potent compound with a higher selective index and CD4 mimicry. The current study identified a novel lead compound **11** with significant anti-HIV activity and lower cytotoxicity than those of known CD4 mimics.

1. Introduction

The dynamic supramolecular mechanism of HIV cellular invasion has emerged as a key target for blocking HIV entry into host cells.[1] HIV entry begins with the interaction of a viral envelope glycoprotein gp120 and a cell surface protein CD4.[2] This triggers extensive conformational changes in gp120 exposing co-receptor binding domains and allowing the subsequent binding of gp120 to a co-receptor, CCR5[3]/CXCR4.[4] Following the viral attachment and co-receptor binding, gp41, another viral envelope glycoprotein mediates the fusion of the viral and cell membranes, thus completing the infection. Molecules interacting with each of these steps are potential candidates for anti-HIV-1 drugs. In particular, discovery and development of novel drugs that inhibit the viral attachment are required for blocking the HIV infection at an early stage.[5]

In 2005, small molecular CD4 mimics targeting the viral attachment were identified by an HIV syncytium formation assay and shown to bind within the Phe43 cavity, a highly conserved pocket on gp120,[6] which is a hydrophobic cavity occupied by the aromatic ring of Phe43 of CD4.[7] These molecules are comprised of three essential moieties: an aromatic ring, an oxalamide linker, and a piperidine ring (Fig. 1) and show micromolar order potency against diverse HIV-1 strains including laboratory and primary isolates. Furthermore, they possess the unique ability to induce the conformational changes in gp120 required for binding with soluble CD4.[8] Such CD4 mimicry can be an advantage for rendering the envelope more sensitive to neutralizing antibodies.[9] While such properties are promising for the development of HIV entry inhibitors and the use combinatorially with neutralizing antibodies, cytotoxicity is one of the drawbacks of CD4 mimics.

To date, we and others have performed structure–activity relationship (SAR) studies of CD4 mimics based on modifications of the aromatic ring, the oxalamide linker, and the piperidine moiety of CD4 mimics. In an initial survey of SAR studies of NBD-556 and NBD-557, Madani et al. revealed that potency (i.e., CD4 binding and mimicry) was highly sensitive to modifications of the aromatic ring, which is thought to bind in the Phe43 cavity of gp120 (Fig. 1). The CD4 mimic analogs (JRC-II-191) with a *para*-chloro-*meta*-fluorophenyl ring had significantly increased affinity for gp120.[10] Our SAR studies also revealed that a certain size and electron-withdrawing ability of the *para*-substituents are indispensable for potent anti-HIV activity.[11] Furthermore, the replacement of the chlorine group at the *para* position with a methyl group which is almost as bulky as a bromine atom leads to improvement of solubility of the compounds in buffer to provide the reproducibility in the biological studies with comparable biological activities.

Further SAR studies were focused on the piperidine moiety of CD4 mimics to investigate its contribution to biological activities, and we found that the piperidine ring is critical for the CD4 mimicry on the conformational changes in gp120 and that substituents on the nitrogen of the piperidine moiety can contribute significantly to both anti-HIV activity and cytotoxicity.[12] Based on these SARs and our modeling study, we speculate that interactions of the piperidine moiety with several amino acids in the vicinity of the Phe43 cavity in gp120, specifically an electrostatic interaction with

* Corresponding author. Tel.: +81 3 5280 8036; fax: +81 3 5280 8039.
E-mail address: tamamura.mr@tmd.ac.jp (H. Tamamura).

0968-0896/$ - see front matter © 2011 Elsevier Ltd. All rights reserved.
doi:10.1016/j.bmc.2011.09.045

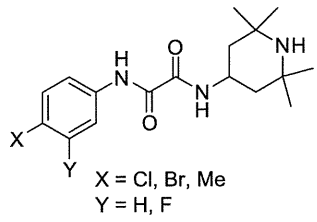

Figure 1. CD4 mimics.

Asp368 and a hydrophobic interaction with Val430, are critical for biological activity. LaLonde et al. focused on modifications of the piperidine moiety using computational approaches, adducing evidence for the importance of these interactions to the binding affinity against gp120.[13] Based on these results, we envisioned that an enhancement of the interaction of CD4 mimics with residues associated with the Phe43 cavity in gp120 would lead to the increase of their potency and CD4 mimicry inducing the conformational changes of gp120, and the decrease of their cytotoxicity. Thus, in this study a series of CD4 mimics, which were designed to interact with the conserved residues in the Phe43 cavity, were synthesized to increase binding affinity for gp120, and the appropriate SAR studies were performed.

2. Results and discussion

Two types of CD4 mimic analogs were designed: (1) CD4 mimics with the ability to interact electrostatically with Asp368, and (2) CD4 mimics with the ability to interact hydrophobically with Val430 (Fig. 2). The X-ray structure of gp120 bound to soluble CD4 (PDB: 1RZJ) revealed that the guanidino group of Arg59 of CD4 is involved in a hydrogen bond with Asp368 of gp120. In order to mimic this interaction, a guanidino and related groups such as thiourea and urea were introduced to the piperidine moiety of the CD4 mimic derivative COC-021, which was developed in order to modify the nitrogen of the piperidine moiety and which showed biological activity, including anti-HIV activity and CD4 mimicry, similar to that of the parent compound NBD-556.[12] Furthermore, to interact with Val430 by hydrophobic interaction, the methyl groups on the piperidine ring were replaced with cyclohexyl groups to prepare a novel CD4 mimic analog with enhanced hydrophobicity.

2.1. Chemistry

The syntheses of CD4 mimics are outlined in Scheme 1. CD4 mimics with guanidine, thiourea, and urea groups on the piperidine moiety were prepared using our previously reported method.[12] Coupling of *p*-chloroaniline with ethyl chloroglyoxylate followed by aminolysis of the ethyl ester with 4-amino-*N*-benzylpiperidine under microwave conditions (150 °C, 3 h) gave the corresponding amide. Removal of the benzyl group with 1-chloroethyl chloroformate[14] gave the free piperidine moiety, which was modified to produce the desired compounds **4–8** (Scheme 1).

For synthesis of a CD4 mimic derivative with two cyclohexyl groups, treatment of 2,2,6,6-tetramethylpiperidin-4-one **9** with cyclohexanone in the presence of ammonium chloride furnished a 2,6-substituted piperidin-4-one derivative,[15] and reductive amination with benzylamine and subsequent removal of benzyl group provided a primary amine **10**. Microwave-assisted aminolysis of ester **2** with amine **10** yielded the desired dicyclohexyl-substituted analog **11** (Scheme 2). The synthesis of the other compounds is described in Supplementary data.

2.2. Biological studies

The anti-HIV activity of synthetic CD4 mimics was evaluated in a single-round viral infective assay. Inhibition of HIV-1 infection was measured as reduction in β-galactosidase gene expression after a single-round of virus infection of TZM-bl cells as described previously.[9] IC_{50} was defined as the concentration that caused a 50% reduction in the β-galactosidase activity (relative light units [RLU]) compared to virus control wells. Cytotoxicity

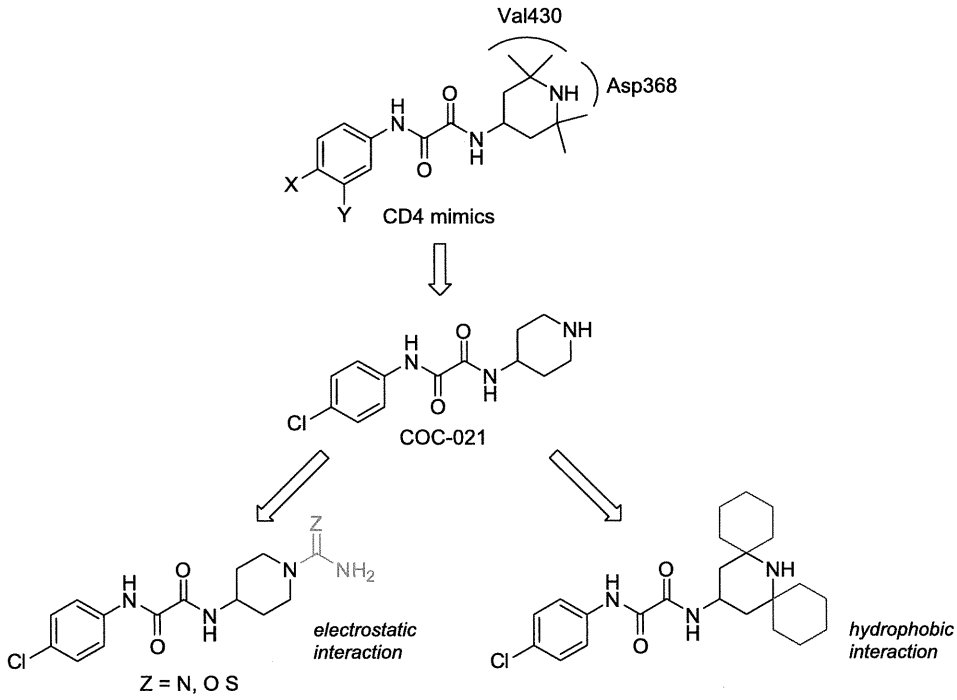

Figure 2. Design strategy for novel CD4 mimics with enhanced electrostatic/hydrophobic interaction.

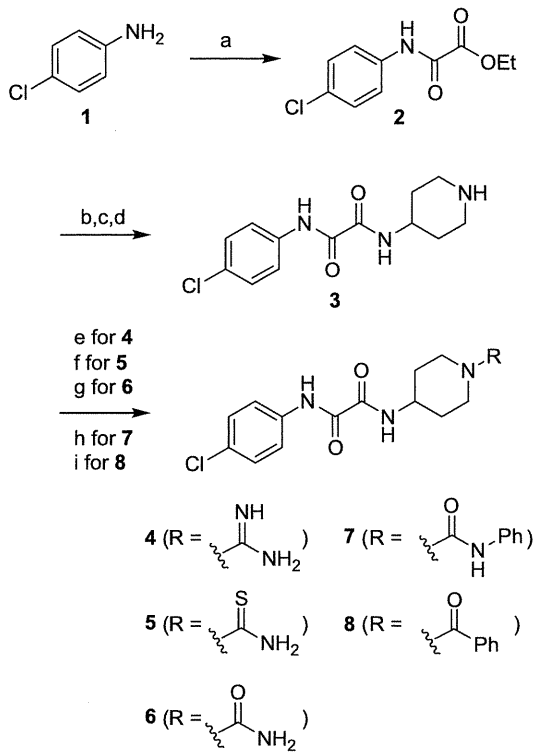

Scheme 1. Synthesis of N-modified piperidine derivatives **4–8**. Reagents and conditions: (a) Ethyl chloroglyoxylate, Et_3N, THF, quant.; (b) 1-benzyl-4-aminopiperidine, Et_3N, EtOH, 150 °C, microwave, 78%; (c) 1-chloroethyl chloroformate, CH_2Cl_2; (d) MeOH, reflux, 64% in two steps; (e) 1*H*-pyrazole-1-carboxamidine hydrochloride, Et_3N, DMF, 61%; (f) (trimethylsilyl)isothiocyanate, $CHCl_3$, 36%; (g) (trimethylsilyl)isocyanate, $CHCl_3$, 30%; (h) phenyl isocyanate, $CHCl_3$, 32%, (i) benzoyl chloride, Et_3N, CH_2Cl_2, 68%.

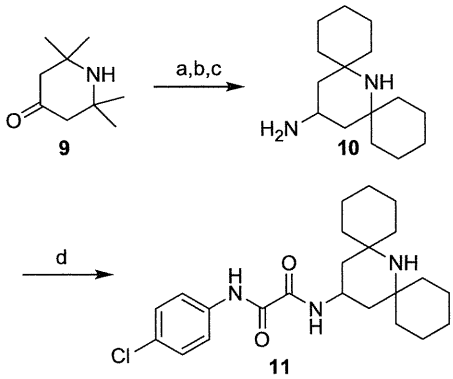

Scheme 2. Synthesis of dicyclohexyl derivative **11**. Reagents and conditions: (a) Cyclohexanone, NH_4Cl, DMSO, 60 °C; (b) benzylamine, $NaBH_4$, MeOH; (c) 10% Pd/C, H_2, MeOH, 7% from **9**; (d) **2**, Et_3N, EtOH, 150 °C, microwave, 17%.

of the compounds based on the viability of mock-infected PM1/CCR5 cells was evaluated using WST-8 method. The assay results for the CD4 mimics **3–8** are shown in Table 1. Compound **12** (NBD-556) showed potent anti-HIV activity; its IC_{50} value was 0.61 μM, and it is thus 13–20-fold more potent than the reported values.[11,12] Although previous studies found that compound **13**, with a methyl group at the *p*-position of the phenyl ring, and compound **3**, with no dimethyl groups on the piperidine ring, showed potent anti-HIV activity, only moderate activities were observed in the current study; this is about 12–14-fold less potency than reported for compound **12** and is probably due to

Table 1
Effects of the nitrogen-substituents on anti-HIV activity and cytotoxicity of CD4 mimic analogs[a]

Compd	X	R	IC_{50}[b] (μM)	CC_{50}[c] (μM)	SI (CC_{50}/IC_{50})
			YTA (R5)		
3[d]	Cl	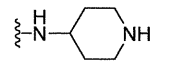	7.0	51	7.3
4[e]	Cl	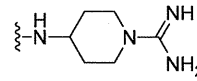	6.1	72	12
5	Cl	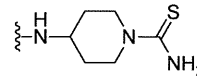	5.5	42	7.6
6	Cl	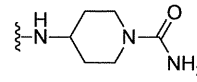	8.3	310	37
7	Cl	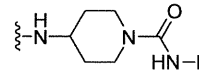	11	6.2	0.56
8	Cl	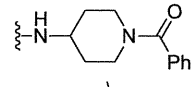	5.1	ND	—
12 (NBD-556)	Cl	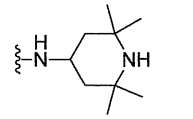	0.61	35	57
13	Me	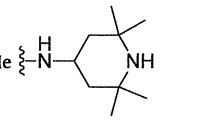	8.4	260	31

[a] All data with standard deviation are the mean values for at least three independent experiments (ND = not determined)
[b] IC_{50} values are based on the reduction in the β-galactosidase activity in TZM-bl cells.
[c] CC_{50} values are based on the reduction of the viability of mock-infected PM1/CCR5 cells.
[d] Desalted by satd $NaHCO_3$ aq.
[e] TFA salts.

the different assay system. All of the synthesized novel derivatives of compound **12** showed moderate to potent anti-HIV activity. A guanidine derivative **4** and thiourea derivative **5** showed potent anti-HIV activities (IC_{50} of **4** = 6.1 μM and IC_{50} of **5** = 5.5 μM) but their potency was approximately 10-fold lower than that of the parent compound **12**. A urea derivative **6** also showed potent anti-HIV activity (IC_{50} = 8.3 μM) and exhibited lower cytotoxicity (CC_{50} = 310 μM). On the other hand, introduction of a phenyl group in the urea derivative **6**, led to an *N*-phenylurea derivative **7**, with an increase of cytotoxicity (CC_{50} = 6.2 μM). To examine the influence of the N–H group on anti-HIV activity, an *N*-benzoyl derivative **8** was also tested. The IC_{50} value of **8** was 5.1 μM, which is equipotent with the thioamide derivative **5**. The *N*-benzoyl derivative **8** was essentially equipotent with **3** and this result suggests the presence of the hydrogen atom of the N–H group does not contribute to an increase in anti-HIV activity. The thiourea derivative **5** and the *N*-phenylurea derivative **7**, which have more acidic protons (pK_a of thiourea and *N*-phenylurea; 21.0 and 19.5,[16] respectively) than the urea derivative **6** (pK_a of urea; 26.9[16]), were found to exhibit relatively strong cytotoxicity. This observation indicates that

Table 2
Anti-HIV activity and cytotoxicity of CD4 mimic analogs **11**, **12**, and **14–17**[a]

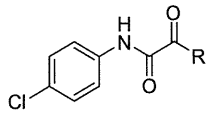

Compd	R	IC_{50}[b] (μM)	CC_{50}[c] (μM)	SI (CC_{50}/IC_{50})
		YTA (R5)		
11	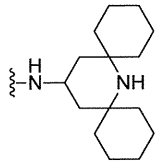	0.68	120	176
14	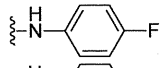	3.1	>500	>160
15	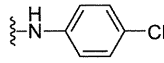	>100	>500	—
16	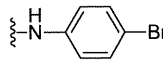	>100	>500	—
17	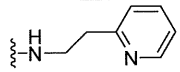	19.8	480	24
12 (NBD-556)	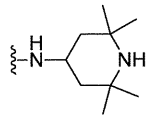	0.61	35	57

[a] All data with standard deviation are the mean values for at least three independent experiments
[b] IC_{50} values are based on the reduction in the β-galactosidase activity in TZM-bl cells.
[c] CC_{50} values are based on the reduction of the viability of mock-infected PM1/CCR5 cells.

substitution on the piperidine moiety of acidic functional groups was unfavorable.

The assay results for CD4 mimics that target hydrophobic interactions are shown in Table 2. Compound **11** showed significant anti-HIV activity (IC_{50} = 0.68 μM) comparable to that of the lead compound **12**, but exhibited lower cytotoxicity. Compound **11** showed approximately four-fold less cytotoxicity than **12**. The SI of **11** is 176, 3 times higher than that of **12** (SI = 57). This result suggests that substitution of bulky hydrophobic groups into the piperidine moiety may be consistent with lower cytotoxicity of CD4 mimics. It is noteworthy that compound **14**, which has a *p*-fluoroanilino group in place of the piperidine ring, exhibits potent anti-HIV activity (IC_{50} = 3.1 μM) without significant cytotoxicity (CC_{50} >500 μM). The SI of compound **14** is >160, which is comparable to that of **11**. However, replacement of the piperidine moiety with a *p*-bromo- or *p*-chloroanilino group resulted in the loss of anti-HIV activity. These results suggest that the introduction of a fluorine atom to the piperidine moiety might be consistent with improvement of the anti-HIV activity. Extension of the alkyl chain by two carbons, as in **17** resulted in a 30-fold loss of anti-HIV activity, indicating that relatively rigid structures are preferable for anti-HIV activity.

The anti-HIV activities of **12** and compound **11**, which has a higher SI than the parent compound **12** were evaluated in a multi-round viral infective assay and the results are shown in Table 3. In this assay, the IC_{50} value of **12** was 0.90 μM, which was slightly larger value than measured in a single-round assay (IC_{50} = 0.61 μM). Compound **11** showed higher anti-HIV activity (IC_{50} = 0.56 μM) than compound **12**, indicating that the introduction of hydrophobic cyclohexyl groups into the piperdine moiety has a positive effect on not only

Table 3
Anti-HIV activity of CD4 mimic **12** and dicyclohexyl derivative **11**[a]

Compd	R	IC_{50}[b] (μM) Single-round assay	IC_{50}[c] (μM) Multi-round assay
12 (NBD-556)	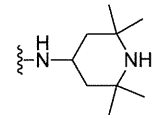	0.61	0.90
11	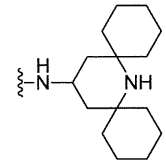	0.68	0.56

[a] All data with standard deviation are the mean values for at least three independent experiments.
[b] IC_{50} values of the single-round assay are based on the reduction in the β-galactosidase activity in TZM-bl cells.
[c] IC_{50} values of the multi-round assay are based on the inhibition of HIV-1-induced cytopathogenicity in PM1/CCR5 cells.

the cytotoxicity but also the anti-HIV activity. This is possibly due to the stability in the assay condition derived from the hydrophobicity of cyclohexyl group(s). These results are consistent with a previous study of the analog with one hydrophobic *gem*-dimethyl group on the piperidine moiety, a compound with potent anti-HIV activity and efficient binding affinity for gp120.[13]

To gain insight into the interactions involved in the binding, molecular modeling of compound **11** docked into gp120 (1RZJ) was carried with Sybyl 7.1 (Fig. 3). The binding mode of compound **11** in the Phe43 cavity suggested that the orientation of the piperidine moiety of **11** is different from that in compound **12**, and that the cyclohexyl group can be positioned near Val430 with whose isopropyl group it can interact hydrophobically.

Fluorescence activated cell sorting (FACS) analysis was performed as previously reported,[11,12] to evaluate the CD4 mimicry effects on conformational changes of gp120 and the results are shown in Figure 4. Comparison of the binding of an anti-envelope CD4-induced monoclonal antibody (4C11) to the cell surface pretreated with the above CD4 mimics was measured in terms of the mean fluorescence intensity (MFI). Our previous studies revealed that the profile of the binding of 4C11 to the Env-expressing cell surface pretreated with compound **12** was entirely similar to that of pretreatment of soluble CD4. In this FACS analysis, the MFI of pretreatment with compound **12** is 23.13. The profiles of the binding of 4C11 to the cell surface pretreated with compounds **3**, **4** and **5** were comparable to that of compound **12** [MFI (**3**) = 20.54, MFI (**4**) = 20.85, MFI (**5**) = 20.24, respectively], suggesting that these derivatives offer a significant enhancement of binding affinity for 4C11. On the other hand, pretreatment with **6** and **8** did not cause significant enhancement of the binding affinity for 4C11, indicating that introduction of a carbonyl group on the piperidine nitrogen is not conducive to CD4 mimicry. The profile of the binding of 4C11 to the Env-expressing cell surface pretreated with compound **11**, which had significant anti-HIV activity and lower cytotoxicity than compound **12**, (MFI (**11**) = 22.17) was similar to that of compound **12**, suggesting that compound **11** offers significant enhancement of binding affinity for 4C11. This result indicates that compound **11** retains the CD4 mimicry on the conformational changes of gp120. Although compound **14** and compound **17** showed potent anti-HIV activity and no significant cytotoxicity, the profiles pretreated with (MFI (**14** and **17**) = 15.20 and 15.38) were similar to that of the control (MFI = 14.94), suggesting that these compounds **14** and **17** failed to produce a significant increase in binding affinity for 4C11. These

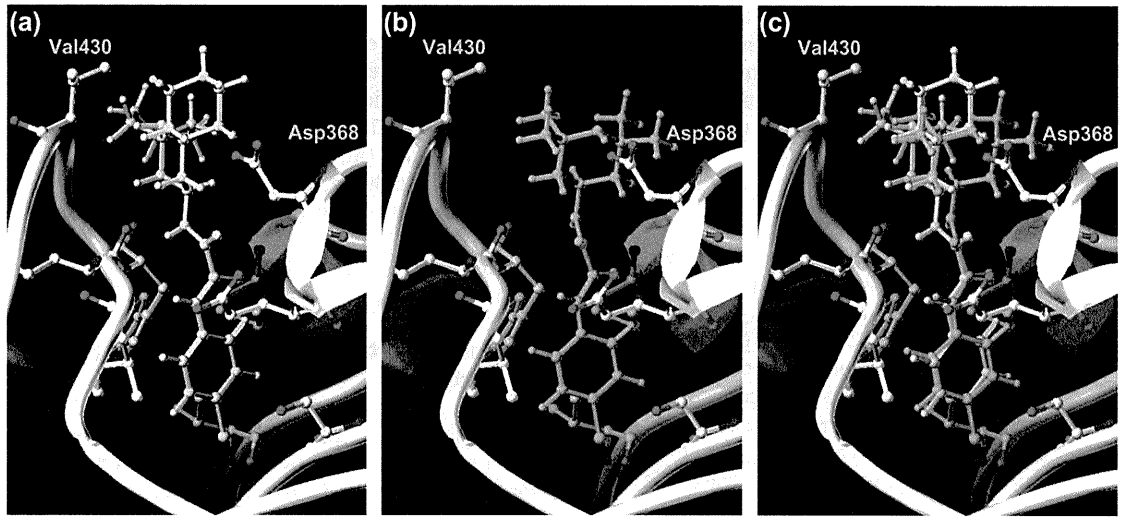

Figure 3. Docking structures of (a) compound **11** and (b) compound **12** bound in the Phe43 cavity of gp120 (1RZJ); (c) merge image of compounds **11** and **12**. Compounds **11** and **12** are represented in yellow and green sticks, respectively. Key residues in the cavity forming interactions with compounds are represented in gray sticks.

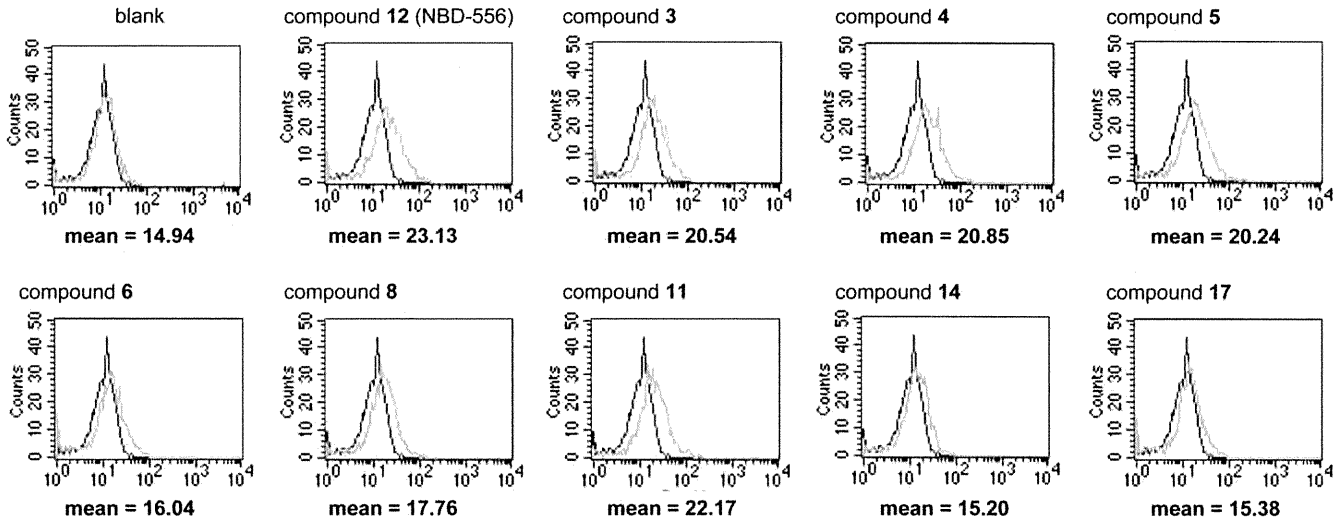

Figure 4. FACS analysis of compounds **12**, **3–6**, **8** (Table 1), **11**, **14**, and **17** (Table 2).

results are consistent with our previous finding that the piperidine ring is critical to the CD4 mimicry of the conformational changes in gp120.

3. Conclusion

A series of CD4 mimics were designed and synthesized to interact with the conserved residues in the Phe43 cavity of gp120 to investigate their anti-HIV activity, cytotoxicity, and CD4 mimicry as a function of conformational change of gp120. The biological activities of the synthetic compounds indicate that (1) the hydrogen atom of the piperidine moieties contributes significantly to cytotoxicity, and (2) installation of bulky hydrophobic groups into the piperidine moiety can increase anti-HIV activity and decrease cytotoxicity thus providing a novel compound with higher selective index than those of the original CD4 mimics. Furthermore, this modification has no great influence on the CD4 mimicry on the conformational change of gp120. Thus, compound **11** is promising for further studies. More detailed SAR investigations with respect to the substitution on the piperidine moiety have been ongoing studies.

4. Experimentals

^{1}H NMR and ^{13}C NMR spectra were recorded using a Bruker Avance III spectrometer. Chemical shifts are reported in δ (ppm) relative to Me_4Si (in $CDCl_3$) as internal standard. Low- and high-resolution mass spectra were recorded on a Bruker Daltonics microTOF focus in the positive and negative detection mode. For flash chromatography, Wakogel C-200 (Wako Pure Chemical Industries, Ltd) and silica gel 60 N (Kanto Chemical Co., Inc.) were employed. For analytical HPLC, a Cosmosil $5C_{18}$-ARII column (4.6 × 250 mm, Nacalai Tesque, Inc., Kyoto, Japan) was employed with a linear gradient of CH_3CN containing 0.1% (v/v) TFA at a flow rate of 1 cm^3 min^{-1} on a JASCO PU-2089 plus (JASCO Corporation, Ltd., Tokyo, Japan), and eluting products were detected by UV at 220 nm. Preparative HPLC was performed using a Cosmosil $5C_{18}$-ARII column (20 × 250 mm, Nacalai Tesque, Inc.) on a JASCO PU-2087 plus (JASCO Corporation, Ltd, Tokyo, Japan) in a suitable